

Optimized auxiliary oscillators for the simulation of general open quantum systems

F. Mascherpa,^{1,*} A. Smirne,¹ D. Tamascelli,^{1,2} P. Fernandez Acebal,¹ S. Donadi,¹ S. F. Huelga,^{1,†} and M. B. Plenio^{1,‡}

¹*Institut für Theoretische Physik, Universität Ulm,
Albert-Einstein-Allee 11, D-89069 Ulm, Germany*

²*Università degli Studi di Milano, Dipartimento di Fisica, Via Celoria 16, I-20133 Milano, Italy*

(Dated: December 15, 2024)

A method for the systematic construction of few-body damped harmonic oscillator networks accurately reproducing the effect of general bosonic environments in open quantum systems is presented. Under the sole assumptions of a Gaussian environment and regardless of the system coupled to it, an algorithm to determine the parameters of an equivalent set of interacting damped oscillators obeying a Markovian quantum master equation is introduced. By choosing a suitable coupling to the system and minimizing an appropriate distance between the two-time correlation function of this effective bath and that of the target environment, the error induced in the reduced dynamics of the system is brought under rigorous control. The interactions among the effective modes provide remarkable flexibility in replicating non-Markovian effects on the system even with a small number of oscillators, and the resulting Lindblad equation may therefore be integrated at a very reasonable computational cost using standard methods for Markovian problems, even in strongly non-perturbative coupling regimes and at arbitrary temperatures including zero. We apply the method to an exactly solvable problem in order to demonstrate its accuracy, and present a study based on current research in the context of coherent transport in biological aggregates as a more realistic example of its use; performance and versatility are highlighted, and theoretical and numerical advantages over existing methods, as well as possible future improvements, are discussed.

I. INTRODUCTION

Any physical system in nature may be studied theoretically in complete isolation from its surroundings. However, since interactions with uncontrolled environmental degrees of freedom are unavoidable in practice, this condition is never actually realized. The effects of said degrees of freedom on the dynamics and general properties of a system are especially important in quantum mechanics, where the time and energy scales involved are likely to make interactions between the system and the surrounding environment a key actor in their own right in the physics at play. The goal of the theory of open quantum systems is to determine the behavior and investigate the physical properties of systems both in and out of equilibrium by properly accounting for environmental effects and other external influences (e.g. driving forces) using appropriate analytical or numerical methods [1–3].

The starting point of such methods may be either a microscopic model for the system and the environment, such as the spin-boson [1, 4], Caldeira–Leggett [5] or more complex models, or an effective description of the system alone with the effects of the environment implicitly taken into account via a quantum master equation [6–12]. The former setup leads to a wide variety of potentially more complete and general treatments, but this greater range of attainable results and predictions comes at moderate to high computational costs [13–19]; the latter construction

is typically less expensive but applies to a constrained class of physical settings, since it either delivers accurate results only in a few well-defined limiting cases [7, 20, 21] or relies on equations which are difficult to derive for general systems [9–12, 22, 23]. Provided that the necessary assumptions on the system–environment interaction are satisfied, however, efficient methods for the solution of the master equation are widely available [24–26].

Much theoretical research in recent decades has focused on the study of complex non-Markovian environments [27–30], for which analytical results are hard to obtain except for specific models, and numerical simulation may become very challenging depending on the physical regime of interest. For thermal bosonic environments, the most commonly studied category by far, numerical methods developed for a general treatment of non-Markovian problems include e.g. Hierarchical Equations of Motion (HEOM) [14, 31], Quasi-Adiabatic Path Integrals (QUAPI) [15, 32–34], Nonequilibrium Green’s Function (NEGF) techniques [13, 35], Non-Markovian Quantum State Diffusion (NMQSD) [18, 19, 36–38], or simulated evolution of the state using the time-adaptive Density Matrix Renormalization Group (t-DMRG) [39–41] in combination with convenient exact mappings of the environment e.g. into one-dimensional oscillator chains well suited for such numerical methods, as in the Time-Evolving Density with Orthogonal Polynomials Algorithm (TEDOPA) [16, 17, 42], to name a few. These methods are often referred to as numerically exact, in the sense that they are designed to address problems from the bottom up, requiring only numerical approximations (e.g. Hilbert space truncation, discretized integrals or finite expansions of relevant functions) in order to keep the costs manageable, but otherwise posing no physical restrictions on

*fabio.mascherpa@uni-ulm.de

†susana.huelga@uni-ulm.de

‡martin.plenio@uni-ulm.de

the models themselves; these numerical errors can sometimes be bounded rigorously, e.g. for TEDOPA [43, 44] or HEOM [45]. Finite bosonic environments [46] can also be used as an approximate treatment for simulation times short enough to prevent recurrence in the dynamics.

An alternative route for the numerical study of such nontrivial open-system problems is to model environmental effects on a system by splitting them into coherent, information-preserving contributions and purely dissipative Markovian damping. Then one can devise effective models in which the system of interest is coupled explicitly to a finite auxiliary system acting as the non-Markovian core of the environment, and dissipation is accounted for through Markovian damping of these auxiliary degrees of freedom. This is the idea underlying approaches such as the pseudomode method [47–50], the reaction-coordinate method [51, 52] or other techniques based on the same concept but differing in the ansatz used to create the effective environment and the techniques to solve for the dynamics [53–56]. Such remappings of open-system problems can be very convenient numerically, but are not always grounded in a mathematically rigorous and physically sound relation between the original and effective environments, making assessment of their accuracy challenging.

In this paper, we present a new approach to general open quantum systems interacting with Gaussian bosonic environments. Our method combines the simplicity and efficiency of simulating a small set of effective degrees of freedom with analytical equivalence relations between the structure and parameters of this auxiliary system and the exact properties of the microscopic environment. Even in cases in which no exact equivalence holds, the physical error from replacing a unitary environment by a dissipative one is kept to a bare minimum and under rigorous control.

Our scheme is based on a quantitatively certified recipe to construct networks of interacting, damped harmonic oscillators specifically designed to mimic any given target environment as specified by its spectral density and temperature. The reduced dynamics is then computed by solving a time-homogeneous quantum master equation of the Gorini–Kossakowski–Sudarshan–Lindblad (GKSL) type [6–8] for the system coupled to these effective harmonic modes and tracing them out at the end. The theoretical foundation underlying this construction lies in a recently proved equivalence theorem between unitary and non-unitary Gaussian environments in open quantum systems [57], which states that the reduced dynamics of a system coupled to an environment of either type is identical if the single-time averages and two-time correlation functions of the environment operators relevant to the interaction are the same. Exploiting this notion, we introduce a systematic procedure by which the effective environment is tailored to reproduce the correlation function of the target environment with an accuracy quantitatively controlled through known error bounds for Gaussian environments [45]. The advantages of the method proposed

are the simple yet versatile structure of the effective environments, which can emulate a broad range of nontrivial unitary environments using small numbers of auxiliary modes, the small, controlled error in the resulting effective dynamics, a high flexibility in the physical regimes which can be studied at comparably low costs, such as high and low temperature and strong as well as weak coupling, and numerical simplicity, since the simulations only require solving a Lindblad equation.

We have organized the presentation of our results as follows: in Section II we will outline the theoretical background and state the equivalence theorem from [57] lying at the core of our method; Section III details the procedure by which an effective environment corresponding to a nontrivial microscopic one may be constructed, and includes an analysis of the theoretical implications and approximations involved; a demonstration of our scheme on the spin-boson model as an exactly solvable test system, with accuracy and performance reports as well as a profile of the numerical advantages and disadvantages of the method in different physical regimes, is given in Section IV; Section V contains an application of the method to a system in a structured environment relevant to current research investigating coherent effects in biomolecular aggregates; in Section VI we discuss the current state of the method, focusing on its scope and applicability, numerical and conceptual strengths and limitations as well as some possible improvements; finally, Section VII summarizes our conclusions and future prospects.

II. THEORETICAL FOUNDATIONS AND SCOPE OF THE METHOD

The non-perturbative method we are going to introduce relies on the equivalence theorem between unitary and dissipative environments stated and proved in [57]; in order to set the stage for discussing our work, we will now introduce the relevant notation, outline the physical context in which the theorem applies and state it explicitly for reference within the paper.

A. Gaussian unitary environments

A wide array of open quantum system (OQS) problems, ranging e.g. from quantum Brownian motion [1, 5] to dissipative cavity and circuit electrodynamics [58, 59] or the study of charge and energy transfer in noisy natural or artificial aggregates [60, 61], can be modeled microscopically by coupling the system of interest to an infinite collection of harmonic oscillators:

$$H := H_S \otimes \mathbb{I}_E + \mathbb{I}_S \otimes H_E + H_I \quad (1)$$

with the free Hamiltonian of the environment

$$H_E := \int_0^\infty d\omega \hbar \omega a_\omega^\dagger a_\omega$$

expressed in terms of creation and annihilation operators obeying the continuum canonical commutation relations $[a_\omega, a_{\omega'}] = 0$, $[a_\omega, a_{\omega'}^\dagger] = \delta(\omega - \omega')$, and a general interaction term of the form [1]

$$H_I := \sum_k A_{S_k} \otimes G_{E_k}.$$

The global state ρ of the system and the environment at time t is determined by the Liouville–Von Neumann equation

$$\frac{d}{dt}\rho(t) = -\frac{i}{\hbar}[H, \rho(t)] \quad (2)$$

and the initial state $\rho_0 := \rho(0)$; the reduced state ρ_S of the system at time t is obtained by taking the partial trace over the environmental degrees of freedom:

$$\rho_S(t) = \text{Tr}_E[\rho(t)]. \quad (3)$$

We are interested in the reduced dynamics of systems interacting with Gaussian environments, i.e. with H_I linear in a_ω and a_ω^\dagger and factorizing initial conditions $\rho_0 = \rho_{0S} \otimes \rho_{0E}$ with ρ_{0E} a Gaussian state. Then the oscillators can be traced out exactly, and the reduced dynamics of the system only depends on the single- and two-time environmental averages $\langle G_{Ek}(t) \rangle_E$ and $C_{kk'}^E(t + \tau, \tau) := \langle G_{Ek}(t + \tau)G_{Ek'}(\tau) \rangle_E$ as given by the evolution of the oscillators with no coupling to the system:

$$\langle G_{Ek}(t) \rangle_E = \text{Tr}_E[U_E^\dagger(t)G_{Ek}U_E(t)\rho_{0E}] \quad (4)$$

$$C_{kk'}^E(t + \tau, \tau) = \text{Tr}_E[U_E^\dagger(t + \tau)G_{Ek}U_E(t)G_{Ek'}U_E(\tau)\rho_{0E}] \quad (5)$$

with $U_E(t) := e^{-iH_E t/\hbar}$.

B. Gaussian dissipative environments

Considering infinite environments evolving unitarily in the absence of a coupled system is one way to bring about dissipation and decoherence in the evolution of the latter when the coupling is nonzero. Alternatively, one may consider finite environments which evolve non-unitarily according to a quantum master equation (QME). In this case, one may start from a Hamiltonian

$$H' := H_S \otimes \mathbb{I}_R + \mathbb{I}_S \otimes H_R + H'_I \quad (6)$$

and a QME describing the evolution of the environment when decoupled from the system:

$$\frac{d}{dt}\rho_R(t) = \mathcal{L}_R[\rho_R(t)] \quad (7)$$

where the new quantum Liouville superoperator

$$\mathcal{L}_R[\rho_R] := -\frac{i}{\hbar}[H_R, \rho_R] + \mathcal{D}_R[\rho_R]$$

includes a dissipator

$$\mathcal{D}_R[\rho_R] := \sum_{i,j=1}^m \Lambda_{ij} \left(L_{Ri}\rho_R L_{Rj}^\dagger - \frac{1}{2} \{L_{Rj}^\dagger L_{Ri}, \rho_R\} \right)$$

with a positive semidefinite rate matrix Λ_{ij} , which makes the dynamics non-unitary but ensures a completely positive and trace-preserving evolution at all positive times. The rate matrix Λ_{ij} , which we take to be constant in time, can always be brought into diagonal form by changing the basis of operators L_{Ri} [1]; this is the quantum dynamical semigroup master equation for Markovian open systems first derived by Gorini, Kossakowski, Sudarshan and Lindblad [6–8]. We will refer to this master equation simply as the Lindblad equation throughout this paper.

The full state of the system and a non-unitary environment evolves according to the QME

$$\frac{d}{dt}\rho(t) = \mathcal{L}[\rho(t)] \quad (8)$$

where

$$\mathcal{L}[\rho] := -\frac{i}{\hbar}[H', \rho] + \mathcal{D}[\rho]$$

is the complete quantum Liouvillian for the system and the environment and $\mathcal{D} := \mathbb{I} \otimes \mathcal{D}_R$ embeds the dissipator \mathcal{D}_R into the full Hilbert space of the problem.

For harmonic environments coupled linearly to the system, i.e. for

$$H_R := \sum_n \hbar\omega_n b_n^\dagger b_n$$

with $[b_m, b_n^\dagger] = \delta_{mn}$ and

$$H'_I := \sum_l A_{Sl} \otimes F_{Rl}$$

with F_{Rl} linear in the creation and annihilation operators, if one also takes the Lindblad operators L_{Ri} linear in b_n and b_n^\dagger and initial conditions $\rho_0 = \rho_{0S} \otimes \rho_{0R}$ with a Gaussian ρ_{0R} then the reduced dynamics of the system will only depend on the environment through $\langle F_{Rl}(t) \rangle_R$ and $C_{ll'}^R(t + \tau, \tau) := \langle F_{Rl}(t + \tau)F_{Rl'}(\tau) \rangle_R$, again considering the free dynamics of the environment with no system attached, like in the unitary case:

$$\langle F_{Rl}(t) \rangle_R = \text{Tr}_R[F_{Rl}e^{\mathcal{L}_R t}[\rho_{0R}]] \quad (9)$$

$$C_{ll'}^R(t + \tau, \tau) = \text{Tr}_R[F_{Rl}e^{\mathcal{L}_R t}[F_{Rl'}e^{\mathcal{L}_R \tau}[\rho_{0R}]]]. \quad (10)$$

Note that the two-time correlation function (10) has the form one would obtain by applying the quantum regression hypothesis [62], which must be handled with some care in general but is true by construction for the Lindblad-damped environments relevant to our work. No approximation is required or implied at this stage [57].

C. Equivalence between unitary and non-unitary environments

While it is clear that if two unitary Gaussian environments share the same averages $\langle G_{Ek}(t) \rangle_E$ and correlation functions $C_{kk'}^E(t + \tau, \tau)$ at all times they will give rise to the same reduced dynamics if coupled to a system, this is not obvious if one or both environments are not unitary. In [57] it was shown, using the unitary dilation formalism for Lindblad equations [2], that this still holds for non-unitary environments under the same conditions. We restate this result here for reference.

Define the reduced dynamics

$$\rho_S^U(t) := \text{Tr}_E[\rho(t)] \quad (11)$$

for some system S coupled to a unitary environment and evolving according to Eq. (2) from factorizing initial conditions with the environment starting in a Gaussian state, and the reduced dynamics

$$\rho_S^L(t) := \text{Tr}_R[\rho(t)] \quad (12)$$

for the same system coupled to a non-unitary environment and evolving according to Eq. (8) from factorizing initial conditions with the environment starting in a Gaussian state.

Both environments are taken to be harmonic and coupled to the system through the same set of A_{Sk} operators in H_I and H'_I , with the corresponding G_{Ek} and F_{Rk} as well as the Lindblad operators L_{Ri} of the non-unitary environment linear in the relevant creation and annihilation operators.

Theorem 1 [57] *Under the above assumptions, if*

$$\langle F_{Rk}(t) \rangle_R = \langle G_{Ek}(t) \rangle_E \quad \forall k, t$$

and

$$C_{kk'}^R(t + \tau, \tau) = C_{kk'}^E(t + \tau, \tau) \quad \forall k, k', t, \tau,$$

then

$$\rho_S^L(t) = \rho_S^U(t) \quad \forall t.$$

This theorem is the cornerstone of our method; for the sake of clarity and an easier understanding of the rest of this paper, some remarks are in order.

First of all, it is important to stress that Gaussianity is a key ingredient of Theorem 1, because in principle all correlation functions up to infinite order would have to be equal for two environments to have the same effect on a system, but for Gaussian environments the single- and two-time functions generate all the others. This restricts the initial state of the environment to the Gaussian family; in this work, we will only consider system-environment product states which are Gaussian in the environmental variables as initial states, leaving the free Hamiltonian, interaction operators and initial density matrix of the system arbitrary.

Furthermore, since no equivalence theorem analogous to Theorem 1 for fermionic or other types of environments is known at the time of writing, we restrict our study to systems coupled to bosonic baths.

Finally, for physical reasons discussed in Section VI and thoroughly analyzed in [63], in general a finite network of damped harmonic oscillators does not yield a two-time correlation function exactly equal to that of an infinite bath, so we will apply the theorem in approximate form by looking for effective parameters such that $C_{kk'}^R(t + \tau, \tau) \approx C_{kk'}^E(t + \tau, \tau)$ and hence $\rho_S^L(t) \approx \rho_S^U(t)$ (single-time expectation values of coupling operators are typically zero or can be set to zero and will no longer be dealt with in this work), relying on the fact that the error in the former approximate relation rigorously bounds that in the latter, as established in previous work [45].

Other than these caveats, no further problems arise in terms of applicability; in particular, temperature and coupling strength between system and environment pose no theoretical or computational limits in principle.

In the next sections we will show how one may exploit the theorem to systematically construct simple networks of damped harmonic oscillators, which can stand in for complex, highly non-Markovian thermal baths at any temperature, by comparing the associated correlation functions (10) and (5). This procedure is independent of the system and the effective environments obtained through it can then be coupled arbitrarily strongly to any system of interest, and standard simulation methods for Lindblad equations may be used to obtain the reduced dynamics at potentially very low computational costs.

III. SYSTEMATIC CONSTRUCTION OF EFFECTIVE ENVIRONMENTS

From now on, we will consider unitary environments with Gaussian stationary states, such as thermal baths, and assume them to be initialized in such states, so that

$$C_{kk'}^E(t + \tau, \tau) = C_{kk'}^E(t, 0),$$

which will be denoted by $C_{kk'}^E(t)$ in the following.

Any harmonic oscillator network obeying a Lindblad equation of the form (7), with \mathcal{L}_R quadratic in b_n and b_n^\dagger , must also start from a stationary ρ_{0R} in order to give a time-homogeneous correlation function matrix $C_{kk'}^R(t) := C_{kk'}^R(t + \tau, \tau) = C_{kk'}^R(t, 0)$ for operators of the form

$$F_{Rk} = \sum_n (c_{nk} b_n + c_{nk}^* b_n^\dagger). \quad (13)$$

The condition for ρ_{0R} to be a stationary state of Eq. (7) is

$$\mathcal{L}_R[\rho_{0R}] = 0. \quad (14)$$

For the initial state of our effective environments, we will therefore need a Gaussian ρ_{0R} satisfying this property.

A. Ansatz and correlation function structure

The correlation functions $C_{kk'}^R(t)$ of the auxiliary environment depend on all parameters appearing in \mathcal{L}_R , ρ_{0R} and the operators F_{Rk} : unrestricted geometries and initial states allow for more generality at the expense of keeping potentially redundant parameters in the model and restricting the range of properties that can be easily calculated; to strike a balance between simplicity and versatility, we will now take an ansatz for the configuration and initial density matrix of the surrogate oscillator network such that the quantities of interest have a simple expression with little loss of generality; for a more extensive discussion of the technical details, we refer the reader to Appendix B.

We choose a free Hamiltonian H_R corresponding to a chain of N oscillators with a hopping interaction between nearest neighbors:

$$H_R := \sum_{n=1}^N \hbar \Omega_n b_n^\dagger b_n + \sum_{n=1}^{N-1} \hbar g_n \left(b_n b_{n+1}^\dagger + b_n^\dagger b_{n+1} \right), \quad (15)$$

where the couplings g_n , as well as one of the coefficients c_{nk} in the interaction operators F_{Rk} appearing in $C_{kk'}^R(t)$, can be assumed real without loss of generality if the F_{Rk} are nonlocal, i.e. acting on all effective modes (see Appendix B). We complete the QME by adding local thermal dissipators at zero temperature acting on each oscillator:

$$\begin{aligned} \frac{d}{dt} \rho_R(t) = & -\frac{i}{\hbar} [H_R, \rho_R(t)] \\ & + \sum_{n=1}^N \Gamma_n \left(b_n \rho_R(t) b_n^\dagger - \frac{1}{2} \{ b_n^\dagger b_n, \rho_R(t) \} \right) \end{aligned} \quad (16)$$

so that the stationary initial state satisfying Eq. (14) is just the overall vacuum state

$$\rho_{0R} = \bigotimes_{n=1}^N |0\rangle\langle 0|_n. \quad (17)$$

Note that a zero-temperature master equation for the effective environment does not restrict the temperature of the target environments it can simulate; the effect of a nonzero temperature in the target bath will simply be encoded in the parameters of the oscillator network, as is done in other approaches [42, 64–67].

The QME (16) and initial condition (17) lead to two decoupled sets of linear equations for $\langle b_n(t) \rangle_R$ and $\langle b_n^\dagger(t) \rangle_R$ related by Hermitian conjugation. For $\langle b_n(t) \rangle_R$ one has

$$\frac{d}{dt} \langle b_n(t) \rangle_R = \sum_{m=1}^N M_{nm} \langle b_m(t) \rangle_R, \quad (18)$$

where

$$M_{nm} := \left(-\frac{\Gamma_n}{2} - i\Omega_n \right) \delta_{nm} - i(g_m \delta_{n, m+1} + g_{m-1} \delta_{n, m-1}). \quad (19)$$

The two-time correlation function $\langle b_n(t) b_m^\dagger(0) \rangle_R$ also evolves according to Eq. (18) as a direct consequence of the quantum regression hypothesis, which holds by construction in this context and states that correlation functions $\langle A(t+\tau) B(t) \rangle$ obey the same equations of motion as the single-time expectation values $\langle A(t+\tau) \rangle$ [2, 68]. This is equivalent to the statement that they can be written in the explicit form given in Eq. (10). Integrating Eq. (18) for $\langle b_n(t) b_m^\dagger(0) \rangle_R$ and plugging the result (as well as its conjugate $\langle b_n^\dagger(t) b_m(0) \rangle_R$, which is identically zero for our initial state (17)) into the expression of $C_{kk'}^R(t)$ in terms of the operators F_{Rk} as given in Eq. (13), one finds

$$C_{kk'}^R(t) = \sum_{n=1}^N (w_n)_{kk'} e^{\lambda_n t} \quad (20)$$

where λ_n are the eigenvalues of the matrix M defined in Eq. (19), which we assume to be non-degenerate for simplicity (see Appendix B for further discussions), and

$$(w_n)_{kk'} = \sum_{l,m=1}^N c_{lk} c_{mk'}^* \mathbf{u}_l^m \mathbf{v}_m^n \quad (21)$$

are complex coefficients obtained from the definition of the operators F_{Rk} and the left and right eigenvectors \mathbf{u}^n and \mathbf{v}^n corresponding to each λ_n , normalized in such a way that $\sum_{l=1}^N \mathbf{v}_l^m \mathbf{u}_l^n = \delta_{mn}$ as discussed in Appendix B. This exponential structure is a consequence of the Lindblad dynamics of the effective environment, which is a requirement of Theorem 1.

B. Transformation to Surrogate Oscillators

Consider an OQS problem described by a microscopic model of the form (1); for simplicity we will now assume a single interaction term, to which there corresponds a correlation function $C^E(t)$. Our goal is to find the matrix elements M_{mn} and operator coefficients c_n of some operator F_R as given in Eq. (13) such that the resulting effective correlation function $C^R(t)$ is as close as possible to $C^E(t)$.

The form of $C^R(t)$ in terms of M_{mn} and c_n is given by Eq. (20), where the eigenvalues λ_n and weights w_n can be thought of as functions of the free parameters Ω_k , g_k , Γ_k and—only the w_n — c_k with $n, k = 1, \dots, N$, where N is the number of oscillators making up the effective bath.

In order to determine the values of these free parameters such that $C^R(t) \approx C^E(t)$, we proceed in two steps. First, we perform a nonlinear fit on $C^E(t)$ using N damped exponentials with complex coefficients

$$C^E(t) \longrightarrow \tilde{C}^E(t) = \sum_{n=1}^N \tilde{w}_n e^{\tilde{\lambda}_n t}, \quad (22)$$

for instance using Prony analysis [69].

Then we solve the problem of matching or getting as close as possible to the $\tilde{\lambda}_n$ and \tilde{w}_n with the $\lambda_n(\Omega_k, g_k, \Gamma_k)$

and $w_n(\Omega_k, g_k, \Gamma_k, c_k)$ from the effective environment. This is in general a highly nontrivial inversion problem involving an underdetermined, non-convex system of nonlinear equations of mixed degrees, and can be hard to solve: there is a trade-off between this complexity and the accuracy of the initial fit, with an optimum at small numbers ($N \leq 5$ in all our applications) of interacting oscillators. Neither existence nor uniqueness of solutions are guaranteed for this inversion problem and physical requirements such as positivity of the rates Γ_n need to be taken into account as well, so it is typically necessary to minimize some distance between $C^R(t)$ and $C^E(t)$ instead of exactly matching the best fit $\tilde{C}^E(t)$; this change in the correlation function is the only error introduced into the problem by the use of an effective environment.

In some cases with $N \leq 3$, it is possible to invert the equations exactly and obtain valid effective bath parameters; we have listed a few explicit solutions in Appendix C and will put some of them to use in our example applications. For general N , we devised a variational recipe to carry out our Transformation to Surrogate Oscillators (TSO) systematically. This is also described in detail in Appendix B and can be summarized as follows:

- Sample random points in a suitably sized open set $(0, g_{\max})^{N-1}$, to be used as coupling constants.
- Substitute each $(N-1)$ -tuple (g_1, \dots, g_{N-1}) into the equations relating the complex eigenvalues λ_n to the $\tilde{\lambda}_n$: this will give rates Γ_n and frequencies Ω_n such that the eigenvalues match; keep only the solutions with all $\Gamma_n > 0$.
- Compute the left and right eigenvectors of the matrices M corresponding to each solution found, plug them into Eq. (21) and minimize a distance (e.g. the Manhattan distance $d_{\text{Man}}(\mathbf{w}, \tilde{\mathbf{w}}) := \sum_{n=1}^N |w_n - \tilde{w}_n|$) between \mathbf{w} and $\tilde{\mathbf{w}}$ by varying the c_n .
- Assess overall accuracy of the solutions found and rank the corresponding $C^R(t)$ according to a meaningful figure of merit, such as the integral $\int_0^t dt' \int_0^{t'} dt'' |C^R(t' - t'') - C^E(t' - t'')|$ from [45].

Effective environments obtained through this procedure can then be used to simulate the reduced dynamics of any model in which the interaction with the bath is mediated by the same bath operator F_R : the TSO is carried out once and for all irrespective of the system coupled to the environment given, and the effective environment can be used in any problem involving the same correlation function $C^E(t)$. We also wish to remark that for composite systems with multiple local environments, the procedure applies to each independent correlation function individually and yields local effective environments to be coupled to the corresponding parts of the system in the same way as the original ones, with no further complications arising; this feature is sketched in Fig. 1.

By the same token, complex correlation functions requiring many exponentials for an accurate fit can be

treated by breaking down the effective environment into smaller clusters of interacting modes, with each cluster accounting for a different component of $C^E(t)$ —or equivalently, the underlying spectral density $J(\omega)$ of the unitary environment—as shown in Fig. 2. Note that decoupling all oscillators from each other, i.e. taking all $g_n = 0$ (which corresponds to requiring all \tilde{w}_n to be real and positive in Eq. (22)), one recovers the noninteracting pseudomodes of [48] as a limiting case.

C. Working example: Ohmic spectral density

To better illustrate the technique explained in the previous subsection, let us now demonstrate how our transformation works with an explicit example.

Consider an arbitrary quantum system coupled to an infinite environment through the position operator of each oscillator (for a more succinct notation, we will leave the tensor products implicit and use natural units $\hbar = 1$, $k_B = 1$ from now on):

$$H = H_S + \int_0^\infty d\omega \omega a_\omega^\dagger a_\omega + A_S \int_0^\infty d\omega g(\omega)(a_\omega + a_\omega^\dagger). \quad (23)$$

This type of coupling for microscopic models is one of the most common in the OQS literature [1, 3–5, 29]. The correlation function of the interaction operator $G_E = \int_0^\infty d\omega g(\omega)(a_\omega + a_\omega^\dagger)$ for a thermal initial state at inverse temperature $\beta = 1/T$ is

$$\begin{aligned} C_\beta^E(t) &= \langle G_E(t)G_E(0) \rangle_{\beta E} \\ &= \int_0^\infty \frac{d\omega}{\pi} J(\omega) \left(\coth\left(\frac{\beta\omega}{2}\right) \cos(\omega t) - i \sin(\omega t) \right) \end{aligned} \quad (24)$$

where the spectral density $J(\omega)$ is related to the frequency-dependent coupling strength $g(\omega)$ through

$$J(\omega) = \pi g^2(\omega)$$

and typically given as a starting point for studying the problem. Spectral densities are real and positive by definition, and are often categorized according to the power of ω best approximating their behavior near the origin, where they are always zero; a $J(\omega) \propto \omega^s$ is called Ohmic if $s = 1$, and super-(sub-)Ohmic if $s > 1$ ($s < 1$). The spectral density and temperature uniquely determine $C_\beta^E(t)$ and, consequently, the effect of the environment on the system.

Note that for unitary environments the correlation function is Hermitian in time, i.e. its real part is even and its imaginary part is odd, as can be seen clearly from Eq. (24). This implies that its Fourier transform

$$\begin{aligned} C_\beta^E(\omega) &= \int_{-\infty}^\infty dt C_\beta^E(t) e^{i\omega t} \\ &= \left(1 + \coth\left(\frac{\beta\omega}{2}\right) \right) (J(\omega)\theta(\omega) - J(-\omega)\theta(-\omega)), \end{aligned} \quad (25)$$

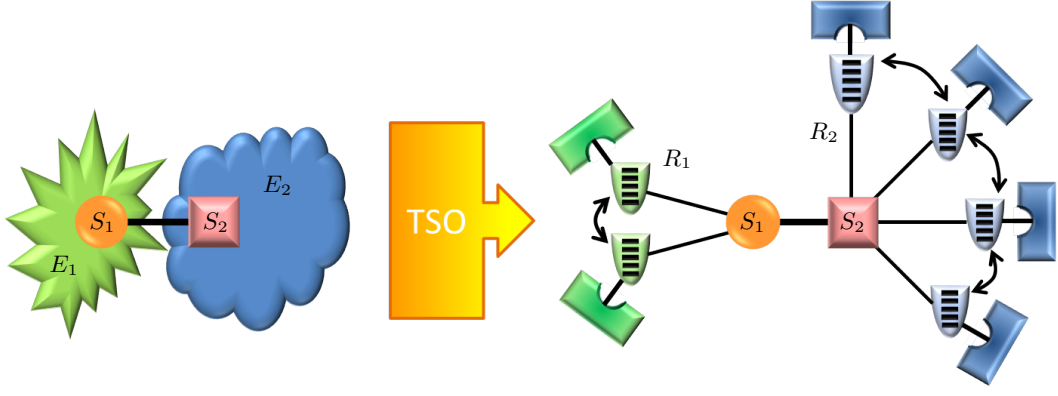


Figure 1: **Simulation of composite systems.** When applying the transformation to surrogate oscillators (TSO) to interacting systems coupled to local environments, each environment is replaced by the corresponding effective one, regardless of the properties of the system attached to it. Our procedure leads to modular structures which do not require a rederivation of the effective parameters when couplings among separate open systems are introduced.

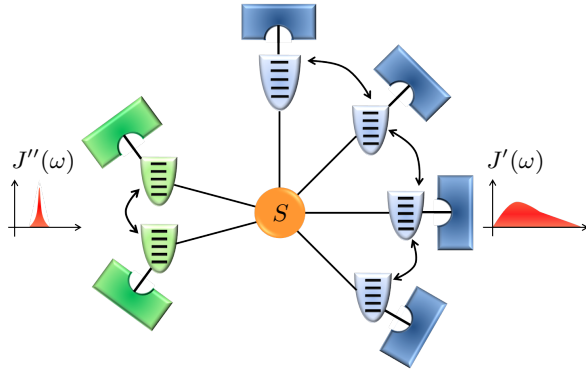


Figure 2: **Simulation of structured environments.** A system coupled to an environment with spectral density $J(\omega) = J'(\omega) + J''(\omega)$, with $J'(\omega)$ a broad background and $J''(\omega)$ a sharp resonance as shown in the small plots, mapped to two distinct effective environments, one with $N = 4$ and another with $N = 2$ oscillators. We will encounter a similar structure in our example application in Section V.

where $\theta(\omega)$ is the Heaviside step function, is always real; at temperature $T = 0$, it is just $2J(\omega)\theta(\omega)$. In fact, $C_\beta^E(\omega)/2$ may itself be regarded as a spectral density defined over a new environment, which encompasses both positive- and negative-frequency modes and gives the correlation function $C_\beta^E(t)$ if initialized in the vacuum [64]: this allows one to effectively rephrase arbitrary-temperature OQS problems as zero-temperature ones if it is convenient to do so, a possibility exploited by thermofield-based and other numerical methods [42, 65–67].

For non-unitary environments, in which time evolution is not an invertible map, correlation functions $C^R(t)$ are only defined at positive times; we extend the definition to negative times by imposing the same symmetry

$$C^R(-t) := C^{R*}(t)$$

in order to be able to compare exact and effective correlation functions in the frequency domain instead of

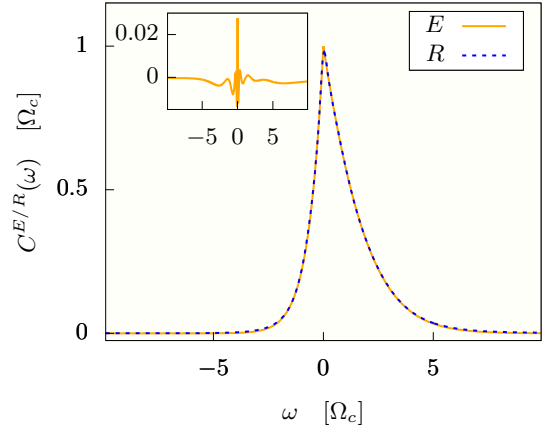


Figure 3: Fourier transform of the Ohmic correlation function $C_\beta^E(t)$ with $\beta\Omega_c = 1$ (solid orange line) and of the corresponding $C_\beta^R(t)$ from the TSO with parameters given in Table I (dashed blue line). The inset shows the difference as a function of frequency.

inspecting their real and imaginary parts separately.

Consider an Ohmic $J(\omega)$ with an exponential cutoff:

$$J(\omega) = \pi\omega e^{-\frac{\omega}{\Omega_c}}. \quad (26)$$

Ohmic spectral densities define a very important class of environments entering the study of many systems, such as a particle undergoing quantum Brownian motion, or microscopic models leading to a Lindblad equation for a harmonic oscillator in a weakly coupled high-temperature environment [1, 5, 70]. The thermal correlation function $C_\beta^E(t)$ corresponding to the spectral density (26) can be determined analytically as

$$C_\beta^E(t) = \frac{\Omega_c^2}{(1 + i\Omega_c t)^2} + \frac{1}{\beta^2} \left(\psi' \left(1 + \frac{1 + i\Omega_c t}{\beta\Omega_c} \right) + \psi' \left(1 + \frac{1 - i\Omega_c t}{\beta\Omega_c} \right) \right) \quad (27)$$

	Mode 1	Mode 2	Mode 3	Mode 4
Ω_n	0.512683	2.53779	4.53293	0.151433
g_n	1.82454	3.20774	1.60194	
Γ_n	0.056336	4.42709	15.7371	0.110104
c_n	-0.962917 +0.819128i	-0.227707 +0.0701249i	0.231179 -0.137866i	0.818093

Table I: Effective parameters for $N = 4$ surrogate modes corresponding to the correlation function of an Ohmic bath at temperature $T = \Omega_c$ (Eq. (27)). All parameters have dimensions of frequency and are given in units of Ω_c ; the last c_n is real.

where $\psi'(z) := \frac{1}{\Gamma(z)} \frac{d\Gamma(z)}{dz}$ is the polygamma function of order one.

Performing our TSO on this correlation function at temperature $T = \Omega_c$ according to the recipe described in the previous subsection, for $N = 4$ we determined the parameters given in Table I; Fig. 3 shows the Fourier-transformed effective correlation function $C_\beta^R(\omega)$ obtained using these parameters and the target $C_\beta^E(\omega)$ for comparison. As can be seen from the plot, four interacting oscillators were enough to obtain a very accurate $C_\beta^R(t)$, with a peak in the error around $\omega = 0$ reaching about 2% of the function value (see the inset of Fig. 3). This error affects the correlation function at very long times compared to its decay time, so we expect it to have a minor impact on the transient reduced dynamics of the system and become potentially more important at very long times. In all our tests, a small region around the origin was consistently found to be the part of the frequency domain where a general $C_\beta^E(\omega)$ is hardest to match: this is because any $C_\beta^R(\omega)$ is analytical around zero by construction, whereas $C_\beta^E(\omega)$ has discontinuous derivatives, as can be checked from Eq. (24). We stress again that the nonzero temperature is encoded in the effective parameters and not in the initial state, allowing us to treat very different temperature regimes at comparable costs, as will be made clearer in the next sections.

IV. A TEST CASE: THE SPIN-BOSON MODEL

We now turn to the second part of our approach: computing the reduced dynamics of a system by coupling it to the effective environment and solving the relevant Lindblad master equation (8).

In order to demonstrate and quantitatively validate the method, we will show here the results we obtained for a system for which an analytical solution is known: the purely dephasing spin-boson model [1, 4, 71]. The Hamiltonian for this system is

$$H = \frac{\omega_0}{2} \sigma_z + \int_0^\infty d\omega \omega a_\omega^\dagger a_\omega + \frac{k}{2} \sigma_z \int_0^\infty d\omega g(\omega) (a_\omega + a_\omega^\dagger) \quad (28)$$

and we consider again the Ohmic spectral density defined in Eq. (26). In this model, the system and interaction Hamiltonians commute and are both diagonal in the sys-

tem basis, so the populations $p_0 := \rho_{00}$ and $p_1 := \rho_{11}$ are conserved by the evolution. Any coherence in this basis present in the initial state, on the other hand, is erased according to the law (see [1] for a derivation)

$$\rho_{01}(t) = \rho_{10}^*(t) = e^{-i\omega_0 t + k^2 \Gamma(t)} \rho_{01}(0) \quad (29)$$

with

$$\Gamma(t) := \int_0^\infty \frac{d\omega}{\pi} J(\omega) \coth\left(\frac{\beta\omega}{2}\right) \frac{\cos(\omega t) - 1}{\omega^2}.$$

Using the cutoff frequency of the environment Ω_c as our energy scale, we set the parameter values $\omega_0 = 4\Omega_c$ and $k = 1$, corresponding to a strong-coupling regime. Comparable coupling strengths appear e.g. in the study of superconducting quantum transmission lines [72]. The system is initialized in the pure state $\rho_{0S} = |+\rangle\langle+|$, with $|+\rangle := \frac{1}{\sqrt{2}}(|0\rangle + |1\rangle)$ in terms of the eigenstates of σ_z , and we simulated the reduced dynamics at three different temperatures $T = 0$, $T = \Omega_c$ and $T = \frac{5}{2}\Omega_c$. Recall that the effective bath is always at zero temperature; different temperatures of the original environment require different surrogate baths. We found accurate effective correlation functions with $N = 4$ for the first two cases, and with $N = 5$ for the high-temperature regime; the parameters are given in Appendix A, and the errors of the two correlation functions at nonzero temperatures are similar to the zero-temperature case already discussed.

A. Results, accuracy and performance

We solved the effective Lindblad equations for all three cases using the QME integrator provided by the Python OQS package QuTiP [73, 74], which implements a twelfth-order Adams-Moulton discrete integration algorithm.

From the results shown in Fig. 4, we see that our simulations with effective correlation functions give quantitatively good results for the coherence $\rho_{01}(t)$ at all times and temperatures (the populations p_0 and p_1 are both equal to 1/2 throughout the evolution), as the overlap between the numerical (solid lines) and exact (dashed lines) solutions shows. The pure quantum decoherence at $T = 0$ induces an algebraic decay asymptotically proportional to t^{-k^2} , while at $T > 0$ the damping becomes exponential; a stronger effective coupling regime, which is determined

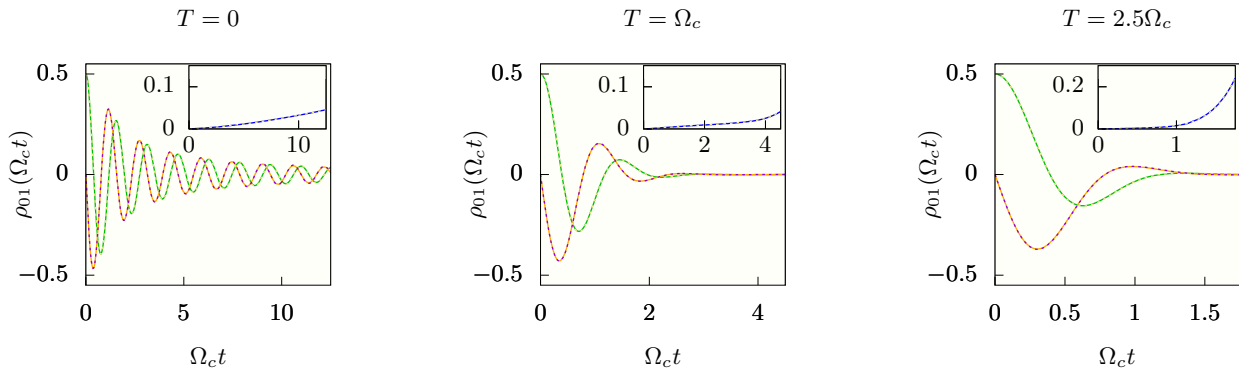


Figure 4: **Spin-boson results.** Time evolution of the density matrix of a qubit starting from the state $\rho_{0S} = |+\rangle\langle+|$, in an Ohmic environment at three different temperatures. The solid lines show the real and imaginary parts of the coherence $\rho_{01}(t)$ obtained by our simulation of the equivalent Lindblad equations, the dashed lines show the analytical solution and the insets show the error as defined in Eq. (30). Both populations are identically 1/2 throughout the evolution and are not shown.

both by k and the strength of thermal effects, induces faster relaxation in the system dynamics.

The plots in the insets show the error figure

$$E_f(t) := \frac{|f(t) - f_{\text{Num}}(t)|}{|f(t)| + |f_{\text{Num}}(t)|}, \quad (30)$$

which is identical for $f = \Re[\rho_{01}]$ (solid line) and $f = \Im[\rho_{01}]$ (dashed line). This is a better estimator for the accuracy of the simulations than e.g. the absolute difference $|f(t) - f_{\text{Num}}(t)|$ because it removes the bias coming from changes in the relaxation time due to temperature, allowing us to compare all regimes on an equal footing. The error, as measured by $E_f(t)$, remains of the order of a few percent until the system has almost reached equilibrium and is comparable for the three regimes probed, mirroring the similar relative errors we had in all three effective correlation functions. The latter observation can be understood as follows: as higher temperatures or larger coupling constants increase the effects of the bath on the system, the error being carried from the correlation function into the reduced dynamics is magnified accordingly; on the other hand, these stronger effective regimes shorten the relaxation time of the system, so the cumulative effect of the error over time is not as severe as when the coupling is weaker or the temperature is lower.

From these results, we conclude that the method is quite reliable and stable provided that the effective correlation functions used are reasonably accurate, and that this accuracy does not command significantly greater effort or complexity in the TSO at higher temperatures and is completely independent of the system and the coupling strength. Furthermore, it is worth noting that any method based on approximating the environment alters its correlation function and is therefore prone to the same kind of error as ours, but we use a rigorously motivated and physically meaningful quantifier to optimize our correlation functions and keep it under control.

The computational cost of the simulations depends on

the local dimension at which each effective mode is truncated and on the spread between the total evolution time and any faster timescales in the problem at hand, though the memory requirements scale faster with the complexity of the problem than the computation times do; to obtain our converged results for this system, which required ~ 4 levels for most oscillators and a maximum of 7 for one mode in each simulation, all running times were below 10 minutes on a laptop. This cost grows rapidly with the number of effective modes, the local dimensions needed for convergence and the size of the system itself; on the other hand, temperature and coupling strength have a limited impact on these factors: a very strong coupling or high temperature will require higher local dimensions but also cause very rapid relaxation to equilibrium, making long simulation times unnecessary. Moreover, when the coupling is stronger and more levels are needed for convergence, this typically affects one particular mode much more than the others, leading to an effective polynomial rather than exponential scaling in the coupling strength and temperature.

V. A PHYSICALLY RELEVANT APPLICATION

Few-body systems non-perturbatively coupled to environments with structured spectra are ubiquitous in many fields ranging from biological physics and chemistry [61, 75] to condensed matter [59, 76] and thermodynamics [77, 78], nanomaterial science and sensing [79] and quantum metrology [80–82], and have prompted much research in theoretical models and numerical methods for non-Markovian OQS. As a first example of an application of our simulation method to a system relevant for current research, we will now show some results for experimentally measurable optical properties in a model inspired by research in coherent charge and energy transfer in biological molecular aggregates [60].

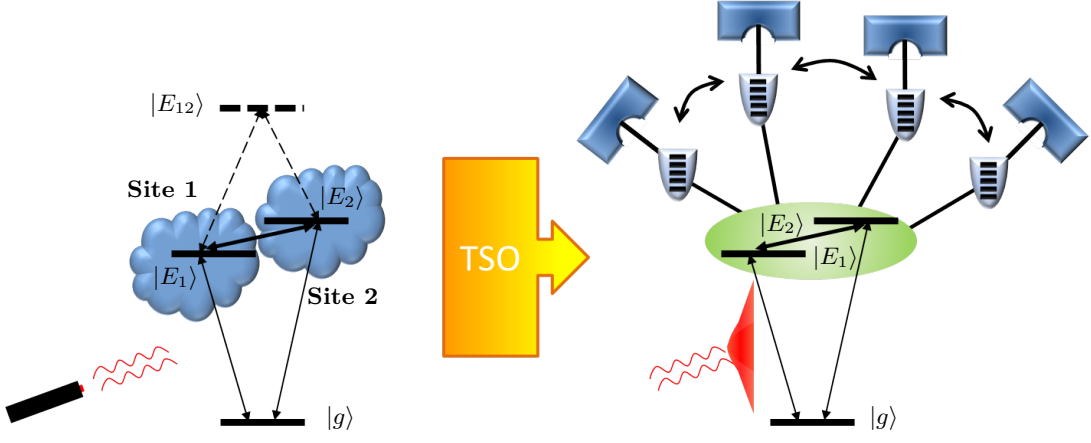


Figure 5: **The dimer model.** Left: the physical picture with the 0-, 1- and 2-excitation subspaces (spanned by the ground state $|g\rangle$, the local excited states $|E_1\rangle$ and $|E_2\rangle$ of the two sites and the doubly excited state $|E_{12}\rangle$, respectively) and independent local environments interacting with each site. Right: the equivalent model after the TSO, with no doubly excited state and a single effective environment corresponding to the relative coordinates as in Eq. (36) and coupled to both local excited states. The wavy lines represent the laser probing a sample in optical experiments.

A. The model

We consider a simple dimer model with system parameters in the range of those found in biomolecular aggregates participating in excitation energy transfer [83, 84], coupled to an environment with a realistic spectral density derived from models common in the literature [85]. We simulated the system and computed its absorption spectrum at temperatures ranging from $T = 0$ K to $T = 300$ K, comparing the results for two different versions of the environmental spectral density in order to identify the optical signatures setting them apart: in particular, we sought to determine the differences between absorption spectra obtained in the presence or absence of a strongly coupled vibrational mode in addition to a broad background spectral density.

Following [84], we considered a free dimer Hamiltonian

$$H_S = E_g |g\rangle\langle g| + \sum_{n=1}^2 E_n |E_n\rangle\langle E_n| + (E_1 + E_2) |E_{12}\rangle\langle E_{12}| + J(|E_1\rangle\langle E_2| + |E_2\rangle\langle E_1|), \quad (31)$$

where the two monomers have on-site energies $E_1 = E_g + 12\,328 \text{ cm}^{-1}$ and $E_2 = E_g + 12\,472 \text{ cm}^{-1}$ and interact through a hopping coefficient $J = 70.7 \text{ cm}^{-1}$, and $|E_{12}\rangle$ is the state with both monomers excited. We assume our system to be probed by a low-intensity laser source, as it is in most absorption experiments [64], and will therefore focus only on optical transitions between the ground state and the single-excitation manifold spanned by the states $|E_n\rangle$, ignoring the doubly excited state $|E_{12}\rangle$ in the following since its contribution is typically negligible. Then, setting $E_g = 0$ as our reference energy, we are left with an effective two-level Hamiltonian for the

single-excitation manifold

$$H_{1\text{ex}} = \sum_{n=1}^2 E_n |E_n\rangle\langle E_n| + J(|E_1\rangle\langle E_2| + |E_2\rangle\langle E_1|), \quad (32)$$

whose eigenstates have an energy gap of $\Delta = 201.8 \text{ cm}^{-1}$.

The local excited states $|E_n\rangle$ interact with separate environments, which account for the molecular vibrations (both within the system and in the protein scaffold around it) and the presence of a solvent. We model these degrees of freedom by coupling the monomers to independent thermal baths with the same spectral density and temperature; the physical model is sketched in the left panel of Fig. 5.

We first studied the problem for a spectral density in the super-Ohmic form introduced by Adolphs and Renger [85]

$$J_{\text{AR}}(\omega) := \frac{\pi}{2 \cdot 9!} \sum_{a=1}^2 \rho_a \frac{\omega^5}{\Omega_{\text{AR}a}^4} e^{-\sqrt{\omega/\Omega_{\text{AR}a}}}, \quad (33)$$

where the two cutoff frequencies are $(\Omega_{\text{AR}1}, \Omega_{\text{AR}2}) = (0.557, 1.936) \text{ cm}^{-1}$ and the weights of the two terms are $(\rho_1, \rho_2) = \frac{288}{5} (\frac{8}{13}, \frac{5}{13})$. This spectral density accounts for environmental noise across a broad frequency range and will be referred to as $J_0(\omega)$ in the following. Then we repeated the analysis for a spectral density featuring a strongly coupled vibrational mode in addition to the broad background: the mode was represented by adding an antisymmetrized Lorentzian peak

$$J_{\text{AL}}(\Omega, \Gamma, S; \omega) := S \frac{8\Gamma\Omega(4\Omega^2 + \Gamma^2)\omega}{(4(\omega - \Omega)^2 + \Gamma^2)(4(\omega + \Omega)^2 + \Gamma^2)}, \quad (34)$$

to the Adolphs–Renger background, and we chose a frequency $\Omega = 200 \text{ cm}^{-1}$, near resonance with the system, a width $\Gamma = 10 \text{ cm}^{-1}$ corresponding to a decay time $(\Gamma/2)^{-1} \sim 1 \text{ ps}$, and a Huang–Rhys factor $S = 0.25$ placing it in a strong-coupling regime with the system. We

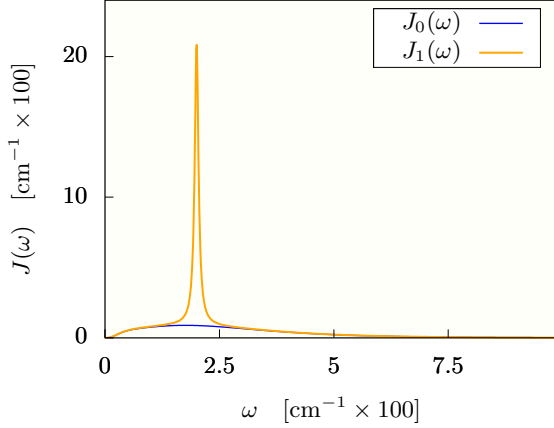


Figure 6: The spectral densities $J_0(\omega)$ and $J_1(\omega)$ of the environments we used in our dimer model.

will refer to the spectral density with the strongly coupled mode as $J_1(\omega)$. The reorganization energies corresponding to the two environments are

$$\lambda_0 = \int_0^\infty \frac{d\omega}{\pi} \frac{J_0(\omega)}{\omega} = \sum_{a=1}^2 \rho_a \Omega_{ARa} = 19.93 \text{ cm}^{-1}$$

$$\lambda_1 = \int_0^\infty \frac{d\omega}{\pi} \frac{J_1(\omega)}{\omega} = \lambda_0 + S\Omega = 69.93 \text{ cm}^{-1}$$

and a plot of both spectral densities is given in Fig. 6.

The total Hamiltonian of our problem

$$H_{\text{tot}} = H_{\text{1ex}} + \sum_{n=1}^2 \int_0^\infty d\omega_n (\omega_n a_{\omega_n}^\dagger a_{\omega_n} + g(\omega_n) |E_n\rangle\langle E_n| (a_{\omega_n} + a_{\omega_n}^\dagger)), \quad (35)$$

can be rewritten in terms of the ‘common-mode’ and ‘relative’ creation and annihilation operators parametrized by a single frequency $A_\omega^{(\dagger)} = \frac{a_{\omega_1}^{(\dagger)} + a_{\omega_2}^{(\dagger)}}{\sqrt{2}}$ and $a_\omega^{(\dagger)} = \frac{a_{\omega_1}^{(\dagger)} - a_{\omega_2}^{(\dagger)}}{\sqrt{2}}$. The common-mode terms then decouple from the system and the Hamiltonian reduces to

$$H = H_{\text{1ex}} + \int_0^\infty d\omega \omega a_\omega^\dagger a_\omega + \frac{1}{\sqrt{2}} (|E_1\rangle\langle E_1| - |E_2\rangle\langle E_2|) \int_0^\infty d\omega g(\omega) (a_\omega + a_\omega^\dagger) \quad (36)$$

in terms of the ‘relative’ modes only. Note that the ground state is decoupled from the single-excitation subspace, since no off-diagonal terms involving it appear in the Hamiltonian (36). The dynamics thus factorizes between the two subspaces unless coherences between them are present in the initial state. A sketch of the model after this rearrangement of the environmental modes and the TSO is given in the right panel of Fig. 5.

Absorption experiments probe the linear response of the system; the light from the laser source can be described as

interacting with the local dipole moment operators $\vec{\mu}_n := \vec{d}_n |E_n\rangle\langle g|$, where \vec{d}_n is the classical dipole moment of the n -th site, in a perturbative manner [64, 68]. Then the spectrum is obtained from the one-sided Fourier transform of the correlation function of the total dipole operator $\vec{\mu} := \sum_{n=1}^2 \vec{\mu}_n$ over the initial stationary state

$$\rho_{0\text{Abs}} := |g\rangle\langle g| \rho_\beta, \quad (37)$$

where the bath is in a thermal state at inverse temperature β and the system is in the electronic ground state, which does not couple to the environment, since excited-state populations at equilibrium are negligible due to the very low intensity of the laser in such a setup [64, 86].

Specifically, the correlation function of interest is given by the scalar product of the dipole operator $\vec{\mu}$, applied at times $t_0 = 0$ and t : in terms of the overall unitary evolution, one has

$$C_\mu(t) := \text{Tr} \left[U^\dagger(t) (\vec{\mu}_1^\dagger + \vec{\mu}_2^\dagger) U(t) \cdot (\vec{\mu}_1 + \vec{\mu}_2) \rho_{0\text{Abs}} \right]. \quad (38)$$

Note that this is formally a two-time object: we can compute it using an effective environment because the first operator acts on the system at equilibrium, so the hypotheses of Theorem 1 are not violated. The unitary dynamics acts on $\tilde{\rho}_0 := (|E_1\rangle + |E_2\rangle)\langle g| \rho_{0\text{Abs}}$, which is still a factorized object with the environment in a thermal state, so the equivalence with a suitable effective Lindblad dynamics remains well defined.

We set the ansatz $\vec{d}_1 = \vec{d}_2 = \vec{d}$ for the geometry of the dimer in order to simplify the form of the dipole correlation function. Normalizing its value to $|\vec{d}|^2$, $C_\mu(t)$ becomes

$$C_\mu(t) = \text{Tr} \left[U^\dagger(t) |g\rangle\langle g| (|E_1\rangle + |E_2\rangle) U(t) (|E_1\rangle + |E_2\rangle)\langle g| \rho_{0\text{Abs}} \right]. \quad (39)$$

The absorption spectrum is then given by

$$S_{\text{Abs}}(\omega) := \omega \Im \lim_{t_{\text{max}} \rightarrow \infty} \int_0^{t_{\text{max}}} dt i C_\mu(t) e^{i\omega t}. \quad (40)$$

B. TSO, results and simulation metrics

In order to calculate $C_\mu(t)$ and hence $S_{\text{Abs}}(\omega)$ for our model, we determined effective parameters for the two spectral densities $J_0(\omega)$ and $J_1(\omega)$ at temperatures $T = 0 \text{ K}$, $T = 77 \text{ K}$ (53.5 cm^{-1}) and $T = 300 \text{ K}$ (208.5 cm^{-1}), performing the TSO separately on the Adolphs–Renger background (33) and the antisymmetrized Lorentzian peak (34). This corresponds to assigning a separate effective environment to each additive part of the spectral density $J_1(\omega)$ and can be a convenient strategy to break down structured spectra, as mentioned in an earlier section and shown in Fig. 2. The effective parameters for the two environments at each temperature are then given by a common set accounting for the background and the extra

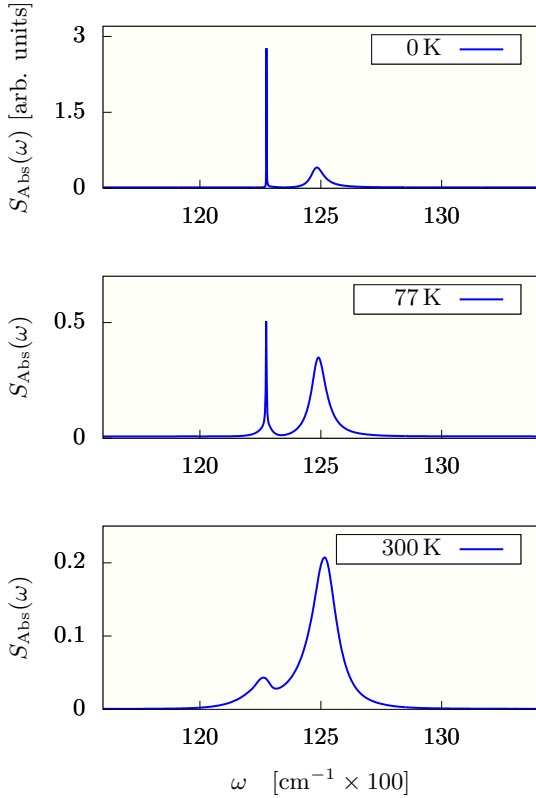


Figure 7: **Absorption spectrum of the dimer with bath spectral density $J_0(\omega)$.** Only the Adolphs–Renger background is present. The absorption maxima appear at the eigenenergies of the system Hamiltonian minus the reorganization energy λ_0 ; the upper eigenstate gives a broader peak, since it can decay to the lower one or lose energy to the bath.

parameters reproducing the peak; the Adolphs–Renger correlation function required $N = 4$ oscillators at all three temperatures, and the Lorentzian mode was replaced by one effective oscillator at $T = 0$ and two interacting ones at $T > 0$ using the exact methods for $N = 1, 2$ described in Appendix C. All parameters of the effective environments are given in Appendix A.

The dipole correlation function can be calculated by solving the effective Lindblad equation with the initial pseudo-state $\tilde{\rho}_0 = (|E_1\rangle + |E_2\rangle)\langle g| \rho_{0\text{Abs}}$. Since the memory required for a direct integration of the equation would become too large for the system coupled to six effective modes with the local dimensions needed for convergence, we carried out the simulations using the quantum jump or Monte Carlo Wave Function (MCWF) method for pure states [25, 87, 88] instead (the memory cost of MCWF scales linearly with the total Hilbert space dimension \mathcal{N} for sparse Lindblad superoperators such as ours, while a master equation integrator requires at least $O(\mathcal{N}^2)$). For correlation functions, a convenient decomposition taking our initial condition $\tilde{\rho}_0$ into account is described in [88]:

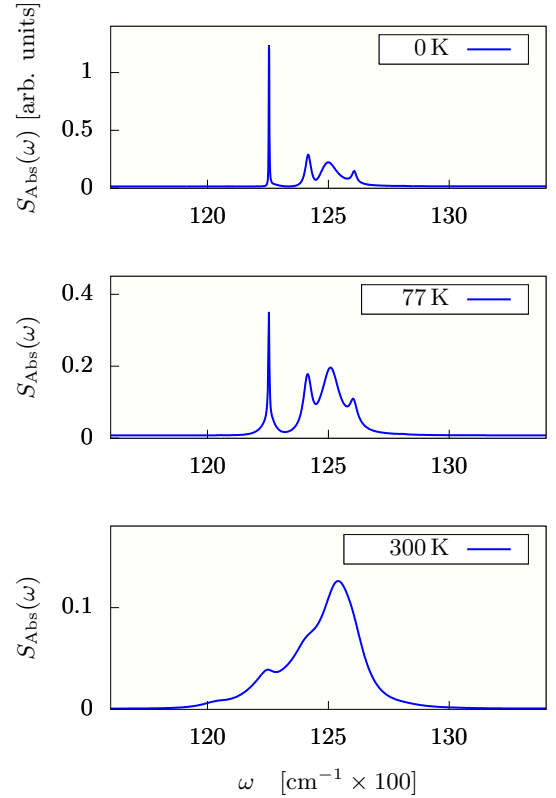


Figure 8: **Absorption spectrum of the dimer with bath spectral density $J_1(\omega)$.** Here a strongly coupled dissipative vibrational mode has been added to the background spectral density. Note the additional spectral lines appearing in the spectrum at frequencies consistent with combined excitations of the system and the mode.

it can be shown that

$$C_\mu(t) = \frac{1}{4} \sum_{k=1}^4 e^{i \frac{k\pi}{2}} \text{Tr} [3 |g\rangle \langle (E_1| + \langle E_2|) | \phi_k(t) \rangle \langle \phi_k(t) |], \quad (41)$$

where for our simulations

$$|\phi_k(0)\rangle := \frac{|g\rangle + e^{-i \frac{k\pi}{2}} (|E_1\rangle + |E_2\rangle)}{\sqrt{3}} |0\rangle_R$$

and the trace is taken over the system and the surrogate modes. The factor 3 appearing in the trace cancels the two normalizations $1/\sqrt{3}$ in the initial states $|\phi_k(0)\rangle \langle \phi_k(0)|$.

The effective Lindblad equation for the system and the modes was solved using another QuTiP code, since the package also provides MCWF routines. Our averages converged after as few as 250 Monte Carlo trajectories for each $|\phi_k(t)\rangle \langle \phi_k(t)|$, i.e. 1000 trajectories in total, due to the jumps occurring in the modes but not in the system (thus partly canceling in the reduced dynamics) and the Fourier transform smearing out the remaining noise over all frequencies; we computed twice as many trajectories as a check but found no visible differences. The results for $J_0(\omega)$ and $J_1(\omega)$ are shown in Figs. 7 and 8, respectively.

T [K]	t_{\max} [ps]	$\frac{ C_\mu(t_{\max}) }{C_\mu(0)}$	
		$J_0(\omega)$	$J_1(\omega)$
0	26.54	$< 10^{-2}$	$< 10^{-3}$
77	13.27	$\sim 10^{-3}$	$< 10^{-3}$
300	1.33	$\sim 10^{-4}$	$< 10^{-4}$

Table II: Total simulation times for the dipole correlation function $C_\mu(t)$ of the dimer and absolute values at the final time for $J_0(\omega)$ and $J_1(\omega)$, respectively.

For each temperature, the system was simulated until the correlation function $C_\mu(t)$ had decayed almost to zero, so that the limit in Eq. (40) could be considered legitimate: the final times we considered in our simulations are reported in Table II.

The absorption spectra obtained via a discrete Fourier transform show the expected features: the result for $J_0(\omega)$ displays absorption lines corresponding to the single-excitation eigenstates $|\varepsilon_{1,2}\rangle$ of $H_{1\text{ex}}$ and appearing at the corresponding energy values redshifted by the bath reorganization energy; the line corresponding to the higher eigenstate is broadened due to the decay channels of that state, which couples to the environment and the lower excited state, whereas the latter gives a very narrow zero-temperature peak since it is not coupled to any lower-lying state it could decay to. At room temperature, the contribution from the upper level becomes larger than the lower one, but the energies associated with the—now markedly broadened—spectral lines no longer represent energy eigenstates of the system, since the system-environment energy eigenbasis is very different from a tensor product basis in this regime, as can be deduced from the fact that the environmental reorganization energy corresponding to the thermalized spectral density $C_\beta^E(\omega)/2$ is comparable to J .

Adding the strong peak to the spectral density, the expected sidebands associated with excitations of both the dimer and the coupled vibrational mode appear for both energy levels; a very small two-phonon sideband of the higher excited state is barely visible to the right of the main spectral curves at lower temperatures but disappears under the strong broadening of the high-temperature spectrum.

It should be noted that the timescale at which the reduced dynamics of the system reaches a steady state is of the order of a few picoseconds for both $J_0(\omega)$ and $J_1(\omega)$ (most of the dissipation is due to the broad Adolphs–Renger background, since the Lorentzian mode has a long lifetime); the decay times of the dipole correlation functions, on the other hand, were found to be very long, especially at low temperatures and if one wants $C_\mu(t)$ to reach values small enough to avoid visible spurious effects from an incomplete decay in the Fourier transform (see again Table II). Such calculations thus require either numerical efficiency up to long simulation times or conditions, such as static disorder, which average out these

long-time effects. Our computational costs scale linearly in the simulation time, making the method suitable for these tasks.

As an extra analysis, we computed the reduced dynamics in the single-excitation subspace for an initial state $\rho_{0S} = |\tilde{\dagger}\rangle\langle\tilde{\dagger}|$, where

$$|\tilde{\dagger}\rangle := \frac{|\varepsilon_1\rangle + |\varepsilon_2\rangle}{\sqrt{2}},$$

for a spectral density $J'_1(\omega)$ combining the background with an attenuated antisymmetrized Lorentzian peak whose parameters are given in Table X in Appendix A. The environmental correlation function at $T = 77$ K and the effective one from the TSO are plotted in Fig. 9, and we computed the reduced dynamics at short times using both our method and the numerically exact TEDOPA [17, 42, 89, 90]. The results are shown in Fig. 10 and confirm the accuracy of our effective Lindblad equation; no comparison was possible for times longer than about 1.3 ps due to the rapidly increasing cost of the TEDOPA simulation at later times.

All simulations required under 3 GB of memory per thread and could therefore have been carried out on a desktop or laptop computer. To achieve higher parallelization of the work, however, we used the JUSTUS cluster at Ulm University: on a 16-cluster node, the simulations with $J_1(\omega)$ took from 27 minutes ($T = 0$ K, $t_{\max} = 26.54$ ps) to 460 minutes ($T = 77$ K, $t_{\max} = 13.27$ ps) per 1000 trajectories; for comparison, analogous calculations (unrelated to this work) for a similar system using TEDOPA take about 60 minutes to reach 0.4 ps and about 90 to reach 0.5 ps on the same hardware, already showing strong nonlinear scaling.

VI. DISCUSSION

After introducing and demonstrating our new simulation method, let us now recapitulate its main theoretical and technical points, discussing its strengths, limitations and error sources in order to give a clear and concise summary of its current state and possible future improvements.

A. Theoretical basis and general remarks

Our method is part of a category of hybrid approaches based on rephrasing microscopic OQS models as effective Markovian problems, in which the memory of the environment is accounted for by an ad hoc auxiliary system. Although this divide-and-conquer strategy between Markovian and non-Markovian effects is a shared feature of several existing methods, the flexibility and quantitative control allowed for by the rigorous theoretical groundwork underlying our construction [45, 57] are, as far as we know, unprecedented for an approach of this type.

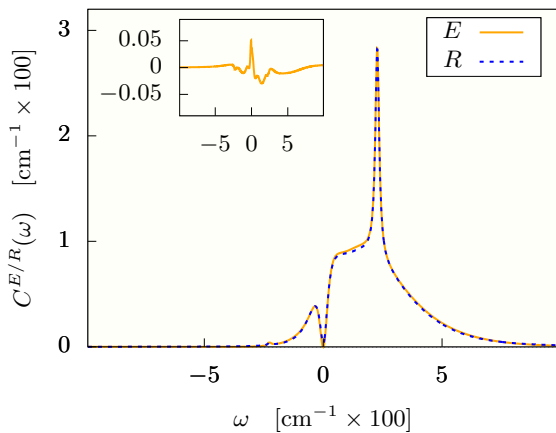


Figure 9: Exact (solid orange line) and effective (dashed blue line) correlation function for $J_1(\omega)$ at $T = 77$ K; four modes were used for the background and two for the peak. The inset shows the TSO error. Note the shape related to the spectral density by Eq. (25), in particular the super-Ohmic dip at frequencies near zero and the mirrored local maxima.

The transformation procedure we described in Section III exploits the generality of the class of mathematically admissible effective environments to tailor them in a systematic way to fit the microscopic ones given: isolating the correlation function as the single property of the environment which needs to be replicated as accurately as possible, we take advantage of the added versatility from using interacting effective modes to make this fitting procedure more accurate while keeping the number of effective degrees of freedom lower than would be possible in chain- or star-configuration schemes. It should be noted that we took one particular ansatz for the effective environment because we found it the most convenient for our needs, but many other choices (non-hopping linear couplings, interactions beyond nearest neighbors, different damping and initial stationary state, etc.) are possible.

Another relevant feature is that the system on which the environment acts does not enter in this part of the procedure at all. Therefore, once the effective parameters corresponding to a given unitary bath are determined, they can be used in all problems which share the same environment: this can be convenient in any field in which standard spectral densities appear in many different situations.

The second part of the method is the simulation of the system coupled to the effective environment. Here any of the analytical or numerical techniques for Lindblad master equations already developed in the literature can be used; the system part of the problem is completely unrestricted, so different strategies can be adopted depending on the problem at hand and available computational resources. We demonstrated the method on two- to three-level systems interacting with small sets of up to six effective modes, for which simple and clear solution methods like direct integration of the master equation or MCWF are

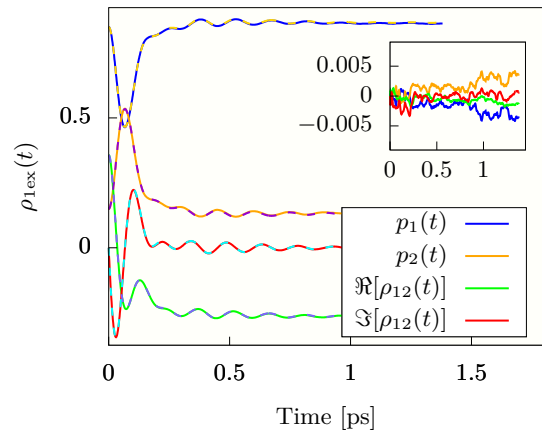


Figure 10: Short-time reduced dynamics in the single-excitation subspace of our dimer model with initial state $\rho_{0S} = |\tilde{+}\rangle\langle\tilde{+}|$ and spectral density $J_1(\omega)$ (defined in the text) at $T = 77$ K, as simulated by our effective Lindblad equation (solid lines, colors as in legend) and TEDOPA (dashed lines). The inset shows the difference between the results.

still suitable.

B. Numerical complexity and costs

As we have shown in the examples given in the preceding sections, our method is very versatile and applies in principle to any non-Markovian, non-perturbative OQS problem involving a Gaussian bosonic bath, at any temperature and coupled arbitrarily strongly to a system. Clearly, some problem classes and physical regimes are more suited than others to this type of treatment: we will now summarize the key elements determining the computational effort for any given application.

Concerning the simulation of systems, the most important variable to look at is the Hilbert space dimension, which includes both the system size and the number and local dimensions of the surrogate modes; temperature and coupling strength, on the other hand, pose less significant challenges. The number of effective oscillators and their parameters come from the TSO and depend on the spectral density and temperature of the unitary environment. The spectral density has a prominent role in determining the number of oscillators required; higher temperatures can contribute too but typically result in an effectively stronger coupling to the system instead: this does cause the oscillators to become more populated, making higher local dimensions necessary for the reduced dynamics to converge, but the added computational cost is usually less than that entailed by adding a new mode. For example, in our application described in the previous section, changing the temperature from 77 K to 300 K required higher local dimensions for three out of six modes, raising them from (6, 5, 6) to (10, 8, 8): the increase in the overall dimension is a factor of about 3.55, i.e. less than that

from adding an oscillator truncated at local dimension 4.

When simulating more complicated systems or environments, the Hilbert space dimensions involved are such that memory, rather than time, typically becomes the main computational concern: such situations are a topic of current relevance in the study of large systems of numerical differential equations [24, 91, 92] and may benefit from ongoing research in the field. For the simulations reported in this paper, with Hilbert space dimensions ranging up to $\sim 3 \cdot 10^5$, the memory required never exceeded 3 GB per thread and we did not need to introduce any Hilbert space optimization beyond truncating the oscillators, but different dimensional reduction schemes such as matrix product operator-based methods [93–95] are a viable alternative when dealing with a large number of degrees of freedom between the system and the oscillators. As for the simulation time, the cost of the method scales linearly in the total evolution time considered whenever the full Hilbert space dimension can be fixed upfront, making it well suited to the study of long-time dynamics and relaxation to equilibrium. When the total effective Hilbert space of a problem is too large and one needs to resort to time-adaptive truncation schemes (such as the aforementioned tensor network-based propagators) in order to compress the memory requirements, this generally results in a nonlinear scaling in time; however, novel methods which can exploit damping in the simulated dynamics to bound the maximum effective dimensions, thus reducing these nonlinear additional costs significantly, are being developed [95] and could greatly boost the computational potential of our approach in problems involving larger systems or many surrogate modes.

As to determining the parameters of the surrogate modes in the first place, the inversion problem from the target correlation function is, in general, a mathematically difficult task. Our TSO algorithm uses a randomized parametrization as a variational method to reduce the number of variables in the problem and unlock a part of the solution, which is then fed back into the inversion problem to determine the values still missing; the solution found is the best possible for the random initial values given, and a minimization on the sample according to a suitable figure of merit is carried out a posteriori.

This rather involved procedure gives satisfactory results but scales poorly with the number of modes; for more than five interacting oscillators, it is already very expensive. This, however, is not a major setback for several reasons. First of all, complex environmental correlation functions typically originate from spectral densities comprising several simple terms, which can be addressed—and recycled for other problems if needed—individually, as demonstrated in our example application; secondly, keeping the number of effective oscillators as low as possible is also a priority for simulation purposes and does not put significant constraints on accessible coupling or temperature regimes; finally, the cost of the TSO is not fixed but depends on the form chosen for the effective environment, so the complexity of our particular algorithm

is not universal.

Possible future improvements to the variational algorithm could come from employing different methods such as simulated annealing or importance sampling in the parameter search or machine-learning techniques to minimize the distance between original and effective correlation functions with respect to the parameters; finding a way to work with the map from effective environment to correlation function in the direct rather than reverse direction, if possible, would be a major simplification.

C. Accuracy and error sources

To complete the discussion of our method, we must now turn to the sources of error affecting the reduced dynamics, and the control we have over them.

The most important error to be addressed is of physical origin and comes from the TSO. This is the error in the correlation function, whose impact on the reduced dynamics and operator expectation values at any time is rigorously bounded [45] (the paper focuses on the spin-boson model in particular, but similar bounds can be derived for other finite systems following the same steps).

Though under control, this error is worth a more careful analysis because it is actually a sum of two errors, one from a fundamental feature of our method, the other from a technical constraint.

The former source is the very form of any correlation function defined as in Eq. (10): it has been shown that no infinite, unitary thermal environment can have a correlation function of the form obtained via the quantum regression formula for a finite, Lindblad-damped auxiliary bath, because the fluctuation-dissipation theorem [1, 96], which holds for continuous, unitary thermal environments, is incompatible, strictly speaking, with the regression hypothesis [63, 97]. This is reflected quantitatively in the fact that no zero-temperature correlation function obtained through the latter is exactly zero on the whole negative frequency domain; however, the violation of the fluctuation-dissipation theorem can always be reduced by adding effective modes, until the unavoidable residual error is comparable to other errors in the model at hand (except in pathological cases, such as the weakly coupled spin-boson model with pure dephasing: this system is only sensitive to the limit of the spectral density at zero frequency, where the analytical differences between unitary and effective environments emerge most clearly, as discussed in Section III).

The second source contributing to the correlation function error are the constraints on the parameters in the master equation: for a fixed number of modes, not every linear combination of complex exponentials can be derived from a valid set of effective bath parameters via Eqs. (20) and (21) (for example, values obtained by setting at least one of the master equation rates Γ_n to a negative value are out of physical scope). Therefore, the closest physically possible correlation function to the one given is generally

not the best unconstrained fit with complex exponentials; however, it is more accurate than the closest fit with the same number of independent pseudomodes, thanks to the added flexibility from the extra coupling parameters.

It should also be mentioned at this point that spectral densities of microscopic models are ultimately derived from experimental results in many applications of current interest [75, 79, 85, 98], so any error in our TSO resulting in a correlation function still compatible with the data is immaterial in practice: any reduced dynamics within the error bounds from [45] given by these differences should be regarded as equally valid.

Finally, the last error source in our method is strictly numerical and comes from the integration schemes used to solve the Lindblad equation, which necessarily involve some truncation of the Hilbert space. This error is not under rigorous control, but requires method-dependent convergence checks like any other numerical solution technique.

D. Impact

Finally, let us sum up the salient features of our simulation method and highlight its distinguishing qualities among existing schemes for general OQS.

First of all, we wish to emphasize that our aim in proposing this approach is to offer the level of accuracy and reliability of a fully microscopic simulation while retaining the benefits of working with two-tiered effective environments, particularly their simple mathematical structure and efficient numerical simulation.

Our scheme fills the gap between exact and simplified effective methods by providing the auxiliary oscillators standing in for any unitary environment with a quantitatively certified link to it, and enables very efficient simulation of nontrivial environments by keeping the number of modes much lower—thanks to the interactions among them—than any similar techniques we are aware of. For example, noninteracting pseudomodes are a special case of our surrogate oscillators, but we found that in order to reproduce an environment such as the one we discussed in our example application in Section V, we would have needed at least 20 pseudomodes to attain the same accuracy given by our TSO with 6 oscillators: while each of our interacting effective modes contributes a term

$$C_n^R(t) = w_n e^{\lambda_n t}$$

with a complex w_n , or

$$C_n^R(\omega) = -2 \frac{\Re[w_n] \Re[\lambda_n] + \Im[w_n](\omega + \Im[\lambda_n])}{\Re[\lambda_n]^2 + (\omega + \Im[\lambda_n])^2},$$

in the frequency domain, to the correlation function, for independent pseudomodes all w_n are real and positive and each $C_n^R(\omega)$ thus becomes just a Lorentzian, which is strictly positive and far less flexible for fitting purposes.

An accurate simulation of our example system with noninteracting pseudomodes would thus have been much more expensive.

We have also compared our simulations with calculations performed using microscopic methods and found that our accuracy is on par with numerically exact results, e.g. from TEDOPA, at least for the relatively simple applications considered in this paper: long-time dynamics are much easier to compute by solving our effective Lindblad equation in all coupling and temperature regimes due to the nonlinear scaling of TEDOPA in the evolution time; on the other hand, spectral densities with complicated shapes requiring a large number of effective oscillators are hard with our method (though the solution of our effective Lindblad equation can be optimized by techniques such as the one presented in [95]) while TEDOPA is much less sensitive to the shape of the spectral density. In our example application, performance was found to be better than TEDOPA at all temperatures for medium to long times (at zero temperature even for very short times) and comparable for short times at nonzero temperature, for a moderately structured spectral density; the scaling in system size and complexity is very similar for the two schemes.

The HEOM method [14, 31] is more akin to our approach in spirit, since it is also based on exponential fitting of $C^E(t)$. Much like our number of surrogate modes, the number of exponentials needed for an adequate fit is the main factor determining complexity of HEOM simulations; although no comparative study was carried out, this number should be the same for the two methods if one requires the same accuracy and uses efficient expansion techniques for the correlation function [99, 100] (these overcome the well-known problem of the more traditional Matsubara-frequency expansion [101, 102], which at low temperatures needs a very large number of exponential terms in order to converge). HEOM scales with the complexity of the spectral density in a similar manner as our method and can likewise account implicitly for temperature through the approximate correlation function. Long evolution times are also not problematic for most regimes; however, they can be in the presence of certain environmental features, e.g. narrow peaks with high Huang–Rhys factors corresponding to strongly coupled environmental modes, which make the hierarchy of equations converge very slowly, significantly increasing the simulation cost. We have shown in our example that including the effect of such terms in our effective baths is not particularly expensive; even higher coupling strengths than we used in that model can be dealt with efficiently. A more quantitative comparison between our effective method and HEOM will be undertaken in another paper.

VII. CONCLUSIONS AND OUTLOOK

We have introduced and demonstrated a new non-perturbative approach for the description and simulation

of arbitrary open quantum systems in Gaussian bosonic environments, which puts no restrictions on temperature, non-Markovianity, system-environment coupling strength or system structure.

Our method is based on the construction of an effective environment of an extremely versatile class, built according to a systematic recipe to capture the effects of any given unitary bath, using as few degrees of freedom as possible and with a clear measure of the error involved. This procedure is grounded in rigorous theoretical results, specifically the equivalence conditions between unitary and dissipative Gaussian environments proved in [57] and the relation between changes in the bath correlation function and in the reduced dynamics and single-time averages of the system given in [45].

The result is a mapping of the problem at hand onto a Lindblad master equation for the system coupled to one or more small networks of interacting effective modes, which can be simulated using standard numerical methods for quantum master equations. The effective modes are always at zero temperature regardless of the temperature of the original environment, giving the Lindblad equation a simple structure, and the interactions among them make a smaller number of modes necessary to account for the specific effect of any given environment than would be the case if they were all independent, with clear computational advantages. Not all modes need to be interacting; environmental spectral densities consisting of several terms may be reproduced using separate clusters of oscillators for each term, simplifying the calculation of their parameters while still exploiting the versatility of interacting oscillators in the rendering of each individual contribution.

As a first example of realistic use, we applied the method to a non-perturbative problem of a kind relevant for current research, obtaining accurate predictions

for experimentally significant quantities across the temperature range from absolute zero to room temperature with desktop-level computational resources. In addition, it was shown that by mapping non-Markovian problems to Markovian ones—provided that the dynamically relevant part of the effective Hilbert space is not too large—the method can deal with short as well as long evolution times at comparable costs, making it a suitable tool for the simulation of long-lived dynamical features and relaxation to equilibrium.

Future work on this project will be aimed mainly at improving the recipe for determining effective environment parameters, enhancing simulation efficiency and carrying out more case studies to better assess accuracy and performance, as well as applications to more systems of theoretical or experimental interest; we also plan to undertake deeper theoretical studies on the properties of mappings between unitary and dissipative environments, in order to determine optimized figures of merit for the effective parameters, gain some insight into system-dependent sensitivity to the error in the correlation function and exploit this knowledge to improve accuracy of the reduced dynamics.

We wish to thank A. Mattioni, F. Caycedo-Soler, J. Lim, A. Somoza, R. Puebla and M. Paternostro for useful discussions, suggestions and feedback about the work presented in this paper. We further acknowledge support by the State of Baden-Württemberg through bwHPC for the use of the BwUniCluster and the German Research Foundation (DFG) through grant no INST 40/467-1 FUGG for the use of the JUSTUS cluster. This work was supported by the ERC Synergy Grant BioQ, the EU Projects HYPERDIAMOND and AsteriQs, and the BMBF projects DiaPol and NanoSpin.

-
- [1] H.-P. Breuer and F. Petruccione. *The theory of open quantum systems*. Oxford University Press, 2002.
 - [2] C. Gardiner and P. Zoller. *Quantum Noise: A Handbook of Markovian and Non-Markovian Quantum Stochastic Methods with Applications to Quantum Optics*. Springer, 2004.
 - [3] U. Weiss. *Quantum Dissipative Systems*. World Scientific, third edition, 2008.
 - [4] A. J. Leggett, S. Chakravarty, A. T. Dorsey, M. P. A. Fisher, A. Garg, and W. Zwerger. Dynamics of the dissipative two-state system. *Reviews of Modern Physics*, 59:1–85, 1987.
 - [5] A. O. Caldeira and A. J. Leggett. Path integral approach to quantum Brownian motion. *Physica A: Statistical Mechanics and its Applications*, 121(3):587–616, 1983.
 - [6] V. Gorini, A. Kossakowski, and E. C. G. Sudarshan. Completely positive dynamical semigroups of N-level systems. *Journal of Mathematical Physics*, 17(5):821–825, 1976.
 - [7] V. Gorini, A. Frigerio, M. Verri, A. Kossakowski, and E. C. G. Sudarshan. Properties of quantum Markovian master equations. *Reports on Mathematical Physics*, 13(2):149–173, 1978.
 - [8] G. Lindblad. On the generators of quantum dynamical semigroups. *Communications in Mathematical Physics*, 48(2):119–130, 1976.
 - [9] S. Nakajima. On quantum theory of transport phenomena: steady diffusion. *Progress of Theoretical Physics*, 20(6):948–959, 1958.
 - [10] R. Zwanzig. Ensemble method in the theory of irreversibility. *The Journal of Chemical Physics*, 33(5):1338–1341, 1960.
 - [11] I. Prigogine. *Non-Equilibrium Statistical Mechanics*. Interscience Publishers, 1962.
 - [12] F. Shibata, Y. Takahashi, and N. Hashitsume. A generalized stochastic Liouville equation. Non-Markovian versus memoryless master equations. *Journal of Statistical Physics*, 17(4):171–187, 1977.
 - [13] J. Rammer and H. Smith. Quantum field-theoretical methods in transport theory of metals. *Reviews of Mod-*

- ern *Physics*, 58:323–359, 1986.
- [14] Y. Tanimura. Nonperturbative expansion method for a quantum system coupled to a harmonic-oscillator bath. *Physical Review A*, 41:6676–6687, 1990.
 - [15] Nancy Makri. Improved Feynman propagators on a grid and non-adiabatic corrections within the path integral framework. *Chemical Physics Letters*, 193(5):435–445, 1992.
 - [16] A. W. Chin, A. Rivas, S. F. Huelga, and M. B. Plenio. Exact mapping between system-reservoir quantum models and semi-infinite discrete chains using orthogonal polynomials. *Journal of Mathematical Physics*, 51(9), 2010.
 - [17] J. Prior, A. W. Chin, S. F. Huelga, and M. B. Plenio. Efficient simulation of strong system-environment interactions. *Physical Review Letters*, 105:050404, 2010.
 - [18] L. Diósi and W. T. Strunz. The non-Markovian stochastic Schrödinger equation for open systems. *Physics Letters A*, 235(6):569–573, 1997.
 - [19] J. Piilo, S. Maniscalco, K. Härkönen, and K.-A. Suominen. Non-Markovian quantum jumps. *Physical Review Letters*, 100:180402, 2008.
 - [20] E. B. Davies. Markovian master equations. *Communications in Mathematical Physics*, 39(2):91–110, 1974.
 - [21] R. Dümcke and H. Spohn. The proper form of the generator in the weak coupling limit. *Zeitschrift für Physik B Condensed Matter*, 34(4):419–422, 1979.
 - [22] A. Smirne and B. Vacchini. Nakajima-Zwanzig versus time-convolutionless master equation for the non-Markovian dynamics of a two-level system. *Physical Review A*, 82:022110, 2010.
 - [23] H.-P. Breuer, B. Kappler, and F. Petruccione. The time-convolutionless projection operator technique in the quantum theory of dissipation and decoherence. *Annals of Physics*, 291:36–70, 2001.
 - [24] B. V. Minchev and W. M. Wright. A review of exponential integrators for first order semi-linear problems, 2005.
 - [25] M. B. Plenio and P. L. Knight. The quantum-jump approach to dissipative dynamics in quantum optics. *Reviews of Modern Physics*, 70:101–144, 1998.
 - [26] N. Gisin and I. C. Percival. The quantum-state diffusion model applied to open systems. *Journal of Physics A: Mathematical and General*, 25(21):5677–5691, 1992.
 - [27] A. Rivas, S. F. Huelga, and M. B. Plenio. Quantum non-Markovianity: characterization, quantification and detection. *Reports on Progress in Physics*, 77(9):094001, 2014.
 - [28] H.-P. Breuer, E.-M. Laine, J. Piilo, and B. Vacchini. Colloquium: Non-Markovian dynamics in open quantum systems. *Reviews of Modern Physics*, 88:021002, 2016.
 - [29] I. de Vega and D. Alonso. Dynamics of non-Markovian open quantum systems. *Reviews of Modern Physics*, 89:015001, 2017.
 - [30] L. Li, M. J. W. Hall, and H. M. Wiseman. Concepts of quantum non-Markovianity: A hierarchy. *Physics Reports*, 759:1–51, 2018.
 - [31] Y. Tanimura and R. Kubo. Time evolution of a quantum system in contact with a nearly Gaussian-Markoffian noise bath. *Journal of the Physical Society of Japan*, 58(1):101–114, 1989.
 - [32] M. Topaler and N. Makri. Quasi-adiabatic propagator path integral methods. Exact quantum rate constants for condensed phase reactions. *Chemical Physics Letters*, 210(1):285–293, 1993.
 - [33] N. Makri and D. E. Makarov. Tensor propagator for iterative quantum time evolution of reduced density matrices. I. Theory. *The Journal of Chemical Physics*, 102(11):4600–4610, 1995.
 - [34] N. Makri and D. E. Makarov. Tensor propagator for iterative quantum time evolution of reduced density matrices. II. Numerical methodology. *The Journal of Chemical Physics*, 102(11):4611–4618, 1995.
 - [35] P. Danielewicz. Quantum theory of nonequilibrium processes, I. *Annals of Physics*, 152(2):239–304, 1984.
 - [36] L. Diósi. Exact semiclassical wave equation for stochastic quantum optics. *Quantum and Semiclassical Optics: Journal of the European Optical Society Part B*, 8(1):309–314, 1996.
 - [37] W. T. Strunz. Linear quantum state diffusion for non-Markovian open quantum systems. *Physics Letters A*, 224(1):25–30, 1996.
 - [38] J. Piilo, K. Härkönen, S. Maniscalco, and K.-A. Suominen. Open system dynamics with non-Markovian quantum jumps. *Physical Review A*, 79:062112, 2009.
 - [39] A. J. Daley, C. Kollath, U. Schollwöck, and G. Vidal. Time-dependent density-matrix renormalization-group using adaptive effective Hilbert spaces. *Journal of Statistical Mechanics: Theory and Experiment*, 2004(04):P04005, 2004.
 - [40] G. Vidal. Efficient simulation of one-dimensional quantum many-body systems. *Physical Review Letters*, 93:040502, 2004.
 - [41] U. Schollwöck. The density-matrix renormalization group. *Reviews of Modern Physics*, 77:259–315, 2005.
 - [42] D. Tamascelli, A. Smirne, S. F. Huelga, and M. B. Plenio. Efficient simulation of finite-temperature open quantum systems. arXiv:1811.12418, in publication.
 - [43] M. P. Woods, M. Cramer, and M. B. Plenio. Simulating bosonic baths with error bars. *Physical Review Letters*, 115:130401, 2015.
 - [44] M. P. Woods and M. B. Plenio. Dynamical error bounds for continuum discretisation via gauss quadrature rules—A Lieb–Robinson bound approach. *Journal of Mathematical Physics*, 57(2):022105, 2016.
 - [45] F. Mascherpa, A. Smirne, S. F. Huelga, and M. B. Plenio. Open systems with error bounds: Spin-boson model with spectral density variations. *Physical Review Letters*, 118:100401, 2017.
 - [46] J. Nokkala, F. Galve, R. Zambrini, S. Maniscalco, and J. Piilo. Complex quantum networks as structured environments: engineering and probing. *Scientific Reports*, 6:26861, 2016.
 - [47] A. Imamoğlu. Stochastic wave-function approach to non-Markovian systems. *Physical Review A*, 50:3650–3653, 1994.
 - [48] B. M. Garraway. Nonperturbative decay of an atomic system in a cavity. *Physical Review A*, 55(3):2290–2303, 1997.
 - [49] B. J. Dalton, Stephen M. Barnett, and B. M. Garraway. Theory of pseudomodes in quantum optical processes. *Physical Review A*, 64:053813, 2001.
 - [50] A. Lemmer, C. Cormick, D. Tamascelli, T. Schaetz, S. F. Huelga, and M. B. Plenio. A trapped-ion simulator for spin-boson models with structured environments. *New Journal of Physics*, 20(7):073002, 2018.
 - [51] J. Iles-Smith, N. Lambert, and A. Nazir. Environmental dynamics, correlations, and the emergence of noncanoni-

- cal equilibrium states in open quantum systems. *Physical Review A*, 90:032114, 2014.
- [52] J. Iles-Smith, A. G. Dijkstra, N. Lambert, and A. Nazir. Energy transfer in structured and unstructured environments: Master equations beyond the Born–Markov approximations. *The Journal of Chemical Physics*, 144(4):044110, 2016.
- [53] A. Fruchtmann, N. Lambert, and E. M. Gauger. When do perturbative approaches accurately capture the dynamics of complex quantum systems? *Scientific Reports*, 6, 2016.
- [54] F. Schwarz, M. Goldstein, A. Dorda, E. Arrigoni, A. Weichselbaum, and J. von Delft. Lindblad-driven discretized leads for nonequilibrium steady-state transport in quantum impurity models: Recovering the continuum limit. *Physical Review B*, 94:155142, 2016.
- [55] I. A. Luchnikov, S. V. Vintskevich, H. Ouerdane, and S. N. Filippov. Simulation complexity of open quantum dynamics: connection with tensor networks. arXiv:1812.00043v2.
- [56] E. Schneider, S. a Beccara, F. Mascherpa, and P. Faccioli. Quantum propagation of electronic excitations in macromolecules: A computationally efficient multiscale approach. *Physical Review B*, 94:014306, 2016.
- [57] D. Tamascelli, A. Smirne, S. F. Huelga, and M. B. Plenio. Nonperturbative treatment of non-Markovian dynamics of open quantum systems. *Physical Review Letters*, 120:030402, 2018.
- [58] B. Yurke and J. S. Denker. Quantum network theory. *Physical Review A*, 29:1419–1437, 1984.
- [59] P. Ribeiro and Vitor R. Vieira. Non-Markovian effects in electronic and spin transport. *Physical Review B*, 92:100302, 2015.
- [60] E. Collini, C. Y. Wong, K. E. Wilk, P. M. G. Curmi, P. Brumer, and G. D. Scholes. Coherently wired light-harvesting in photosynthetic marine algae at ambient temperature. *Nature*, 463:644, 2010.
- [61] S. F. Huelga and M. B. Plenio. Vibrations, quanta and biology. *Contemporary Physics*, 54(4):181–207, 2013.
- [62] M. Lax. Formal theory of quantum fluctuations from a driven state. *Physical Review*, 129:2342–2348, 1963.
- [63] P. Talkner. The failure of the quantum regression hypothesis. *Annals of Physics*, 167(2):390–436, 1986.
- [64] V. May and O. Kühn. *Charge and energy transfer dynamics in molecular systems*. John Wiley & Sons, 2008.
- [65] I. de Vega and M. C. Bañuls. Thermofield-based chain-mapping approach for open quantum systems. *Physical Review A*, 92:052116, 2015.
- [66] L. Diósi, N. Gisin, and W. T. Strunz. Non-Markovian quantum state diffusion. *Physical Review A*, 58:1699–1712, 1998.
- [67] G. Ritschel, D. Suess, S. Möbius, W. T. Strunz, and A. Eisfeld. Non-Markovian quantum state diffusion for temperature-dependent linear spectra of light harvesting aggregates. *The Journal of Chemical Physics*, 142(3):034115, 2015.
- [68] H. Carmichael. *An Open Systems Approach to Quantum Optics*. Springer, 1993.
- [69] S. L. Marple. *Digital spectral analysis: with applications*, volume 5. Prentice-Hall Englewood Cliffs, NJ, 1987.
- [70] G. W. Ford, J. T. Lewis, and R. F. O’Connell. Independent oscillator model of a heat bath: Exact diagonalization of the Hamiltonian. *Journal of Statistical Physics*, 53(1):439–455, 1988.
- [71] A. O. Caldeira and A. J. Leggett. Influence of damping on quantum interference: An exactly soluble model. *Physical Review A*, 31(2):1059–1066, 1985.
- [72] B. Peropadre, D. Zueco, D. Porras, and J. J. García-Ripoll. Nonequilibrium and nonperturbative dynamics of ultrastrong coupling in open lines. *Physical Review Letters*, 111:243602, 2013.
- [73] J. R. Johansson, P. D. Nation, and F. Nori. QuTiP: An open-source Python framework for the dynamics of open quantum systems. *Computer Physics Communications*, 183(8):1760–1772, 2012.
- [74] J. R. Johansson, P. D. Nation, and F. Nori. QuTiP 2: A Python framework for the dynamics of open quantum systems. *Computer Physics Communications*, 184(4):1234–1240, 2013.
- [75] K. M. Pelzer, A. F. Fidler, G. B. Griffin, S. K. Gray, and G. S. Engel. The dependence of exciton transport efficiency on spatial patterns of correlation within the spectral bath. *New Journal of Physics*, 15(9):095019, 2013.
- [76] J. F. Haase, P. J. Vetter, T. Unden, A. Smirne, J. Roskopf, B. Naydenov, A. Stacey, F. Jelezko, M. B. Plenio, and S. F. Huelga. Controllable non-Markovianity for a spin qubit in diamond. *Physical Review Letters*, 121:060401, 2018.
- [77] R. Uzdin, A. Levy, and R. Kosloff. Quantum heat machines equivalence, work extraction beyond Markovianity, and strong coupling via heat exchangers. *Entropy*, 18(4), 2016.
- [78] M. T. Mitchison and M. B. Plenio. Non-additive dissipation in open quantum networks out of equilibrium. *New Journal of Physics*, 20(3):033005, 2018.
- [79] Y. Wu, F. Jelezko, M. B. Plenio, and T. Weil. Diamond quantum devices in biology. *Angewandte Chemie International Edition*, 55(23):6586–6598, 2016.
- [80] A. W. Chin, S. F. Huelga, and M. B. Plenio. Quantum metrology in non-Markovian environments. *Physical Review Letters*, 109:233601, 2012.
- [81] A. Smirne, J. Kołodyński, S. F. Huelga, and R. Demkowicz-Dobrzański. Ultimate precision limits for noisy frequency estimation. *Physical Review Letters*, 116:120801, 2016.
- [82] J. F. Haase, A. Smirne, J. Kołodyński, R. Demkowicz-Dobrzański, and S. F. Huelga. Fundamental limits to frequency estimation: a comprehensive microscopic perspective. *New Journal of Physics*, 20(5):053009, 2018.
- [83] M. B. Plenio and S. F. Huelga. Dephasing-assisted transport: quantum networks and biomolecules. *New Journal of Physics*, 10(11):113019, 2008.
- [84] M. B. Plenio, J. Almeida, and S. F. Huelga. Origin of long-lived oscillations in 2D-spectra of a quantum vibronic model: Electronic versus vibrational coherence. *The Journal of Chemical Physics*, 139(23):235102, 2013.
- [85] J. Adolphs and T. Renger. How proteins trigger excitation energy transfer in the FMO complex of green sulfur bacteria. *Biophysical Journal*, 91(8):2778–2797, 2006.
- [86] S. Mukamel. *Principles of Nonlinear Optical Spectroscopy*. Oxford University Press, 1995.
- [87] R. Dum, P. Zoller, and H. Ritsch. Monte Carlo simulation of the atomic master equation for spontaneous emission. *Physical Review A*, 45:4879–4887, 1992.
- [88] J. Dalibard, Y. Castin, and K. Mølmer. Wave-function approach to dissipative processes in quantum optics. *Physical Review Letters*, 68:580–583, 1992.

- [89] D. Tamascelli, R. Rosenbach, and M. B. Plenio. Improved scaling of time-evolving block-decimation algorithm through reduced-rank randomized singular value decomposition. *Physical Review E*, 91:063306, 2015.
- [90] L. Kohn, F. Tschirsich, M. Keck, M. B. Plenio, D. Tamascelli, and S. Montangero. Probabilistic low-rank factorization accelerates tensor network simulations of critical quantum many-body ground states. *Physical Review E*, 97:013301, 2018.
- [91] H. D. Vo and Roger B. Sidje. Approximating the large sparse matrix exponential using incomplete orthogonalization and Krylov subspaces of variable dimension. *Numerical Linear Algebra with Applications*, 24(3):e2090, 2017.
- [92] S. Gaudreault, G. Rainwater, and M. Tokman. KIOPS: A fast adaptive Krylov subspace solver for exponential integrators. *Journal of Computational Physics*, 372:236–255, 2018.
- [93] E. Mascarenhas, H. Flayac, and V. Savona. Matrix-product-operator approach to the nonequilibrium steady state of driven-dissipative quantum arrays. *Physical Review A*, 92:022116, 2015.
- [94] J. Cui, J. I. Cirac, and M. C. Bañuls. Variational matrix product operators for the steady state of dissipative quantum systems. *Physical Review Letters*, 114:220601, 2015.
- [95] A. D. Somoza, O. Marty, J. Lim, S. F. Huelga, and M. B. Plenio. Dissipation-assisted matrix product factorization. arXiv:1903.05443.
- [96] H. B. Callen and T. A. Welton. Irreversibility and generalized noise. *Physical Review*, 83:34–40, 1951.
- [97] G. W. Ford and R. F. O’Connell. There is no quantum regression theorem. *Physical Review Letters*, 77:798–801, 1996.
- [98] D. I. G. Bennett, P. Malý, C. Kreisbeck, R. van Grondelle, and A. Aspuru-Guzik. Mechanistic regimes of vibronic transport in a heterodimer and the design principle of incoherent vibronic transport in phycobiliproteins. *The Journal of Physical Chemistry Letters*, 9(10):2665–2670, 2018. PMID: 29683676.
- [99] C. Duan, Q. Wang, Z. Tang, and J. Wu. The study of an extended hierarchy equation of motion in the spin-boson model: The cutoff function of the sub-Ohmic spectral density. *The Journal of Chemical Physics*, 147(16):164112, 2017.
- [100] C. Duan, Z. Tang, J. Cao, and J. Wu. Zero-temperature localization in a sub-ohmic spin-boson model investigated by an extended hierarchy equation of motion. *Physical Review B*, 95:214308, 2017.
- [101] C. Meier and D. J. Tannor. Non-Markovian evolution of the density operator in the presence of strong laser fields. *The Journal of Chemical Physics*, 111(8):3365–3376, 1999.
- [102] J. Hu, M. Luo, F. Jiang, R.-X. Xu, and Y. Yan. Padé spectrum decompositions of quantum distribution functions and optimal hierarchical equations of motion construction for quantum open systems. *The Journal of Chemical Physics*, 134(24):244106, 2011.

Appendix A: Effective parameters

We list here several sets of effective parameters used in the simulations discussed in the main text, along with the local dimensions of each mode in each set at convergence. The corresponding spectral densities are defined in Eq. (26), Eq. (33) and Eq. (34) of the main text, respectively.

Ohmic spectral density

	Mode 1	Mode 2	Mode 3	Mode 4
Ω_n	2.70796	2.13014	1.15884	0.310906
g_n	3.38195	1.43514	0.491546	
Γ_n	11.9298	0.573494	0.0317143	0.000795693
c_n	-0.0333215 -0.0121362 <i>i</i>	0.319 +0.0811955 <i>i</i>	0.760716 +0.0175762 <i>i</i>	0.579218
d_{loc}	3	4	5	7

Table III: Ohmic spectral density with cutoff frequency Ω_c , temperature $T = 0$: parameters in units Ω_c and local dimensions.

	Mode 1	Mode 2	Mode 3	Mode 4
Ω_n	0.512683	2.53779	4.53293	0.151433
g_n	1.82454	3.20774	1.60194	
Γ_n	0.056336	4.42709	15.7371	0.110104
c_n	-0.962917 +0.819128 <i>i</i>	-0.227707 +0.0701249 <i>i</i>	0.231179 -0.137866 <i>i</i>	0.818093
d_{loc}	5	4	4	7

Table IV: Ohmic spectral density with cutoff frequency Ω_c , temperature $T = \Omega_c$: parameters in units Ω_c and local dimensions.

	Mode 1	Mode 2	Mode 3	Mode 4	Mode 5
Ω_n	0.306859	0.361308	0.167597	0.0297981	0.00236395
g_n	4.17718	2.1243	0.673391	0.166947	
Γ_n	16.0093	2.76375	0.00358704	0.0949691	0.0517414
c_n	-0.166675 -0.0342019 <i>i</i>	0.21927 +0.103791 <i>i</i>	1.61933 -0.00703994 <i>i</i>	0.187388 -1.07416 <i>i</i>	1.1553
d_{loc}	3	3	4	4	6

Table V: Ohmic spectral density with cutoff frequency Ω_c , temperature $T = \frac{5}{2}\Omega_c$: parameters in units Ω_c and local dimensions.

Adolphs–Renger spectral density

	Mode 1	Mode 2	Mode 3	Mode 4
Ω_n	0.718918	3.06543	2.96082	0.667101
g_n	2.10958	3.91248	1.56527	
Γ_n	0.00554063	15.4881	0.00291091	0.294244
c_n	-0.57271 +0.06491 <i>i</i>	-0.0147923 +0.0820348 <i>i</i>	0.725729 +0.0119678 <i>i</i>	0.409762
d_{loc}	6	4	4	4

Table VI: Adolphs–Renger spectral density, temperature $T = 0$: parameters in units $u = 100 \text{ cm}^{-1}$ and local dimensions.

	Mode 1	Mode 2	Mode 3	Mode 4
Ω_n	3.05106	2.74196	0.00670418	0.00780109
g_n		2.74161	2.01796	0.33975
Γ_n	0.0284151	11.6481	0.00549033	0.0184315
c_n	-0.910465 -0.0164266 <i>i</i>	-0.135049 -0.0104797 <i>i</i>	0.524001 +0.317767 <i>i</i>	0.114767
d_{loc}	5	4	6	8

Table VII: Adolphs–Renger spectral density, temperature $T = 77$ K: parameters in units $u = 100 \text{ cm}^{-1}$ and local dimensions.

	Mode 1	Mode 2	Mode 3	Mode 4
Ω_n	0.788783	0.414407	-0.0300357	-0.034035
g_n		3.10576	0.978945	0.294823
Γ_n	10.4575	0.0934767	0.00983292	0.0167273
c_n	0.189405 +0.0639657 <i>i</i>	1.23326 +0.451035 <i>i</i>	0.0221509 +0.962709 <i>i</i>	0.365249
d_{loc}	4	5	10	8

Table VIII: Adolphs–Renger spectral density, temperature $T = 300$ K: parameters in units $u = 100 \text{ cm}^{-1}$ and local dimensions.

Antisymmetrized Lorentzian spectral densities

	$T = 0$ K	$T = 77$ K		$T = 300$ K	
		Mode 1	Mode 2	Mode 1	Mode 2
Ω_n	2.00	-0.318699	0.316331	-0.00048954	0.000480821
g_n	–		1.976		2.00052
Γ_n	0.098296	0.045988	0.138442	0.00953908	0.190362
c_n	0.992322	0.764199 +0.000002 <i>i</i>	0.676024	1.45733 +0.000003 <i>i</i>	0.343374
d_{loc}	6	5	6	8	8

Table IX: Antisymmetrized Lorentzian spectral density with $\Omega = 200 \text{ cm}^{-1}$, $\Gamma = 10 \text{ cm}^{-1}$, $S = 0.25$ from $J_1(\omega)$: parameters in units $u = 100 \text{ cm}^{-1}$ and local dimensions.

	$T = 0$ K	$T = 77$ K		$T = 300$ K	
		Mode 1	Mode 2	Mode 1	Mode 2
Ω_n	2.275	0.662126	-0.667153	-0.00139464	0.0013106
g_n	–		2.1788		2.2772
Γ_n	0.197195	0.264596	0.0788813	0.00326568	0.396252
c_n	0.440408	0.333222 -0.000005 <i>i</i>	0.296358	0.578109 -0.176482 <i>i</i>	0.169995
d_{loc}	5	4	4	4	4

Table X: Antisymmetrized Lorentzian spectral density with $\Omega = 227.5 \text{ cm}^{-1}$, $\Gamma = 20 \text{ cm}^{-1}$, $S = 0.0379$ from $J'_1(\omega)$: parameters in units $u = 100 \text{ cm}^{-1}$ and local dimensions.

Appendix B: Transformation to Surrogate Oscillators in detail

In Section III of the main text, we defined the general form of the effective environments used in our method, and sketched the transformation algorithm by which we obtain their parameters given a target correlation function. Here we will go through the procedure in detail, in order to give a clearer view of its more technical aspects.

1. Effective correlation function

The Hamiltonian for our effective oscillators in a chain configuration with hopping interactions is (with $\hbar = 1$)

$$H_R := \sum_{n=1}^N \Omega_n b_n^\dagger b_n + \sum_{n=1}^{N-1} \left(g_n b_n b_{n+1}^\dagger + g_n^* b_n^\dagger b_{n+1} \right) \quad (\text{B1})$$

and we consider a zero-temperature Lindblad dissipator

$$\mathcal{D}_R[\rho_R] := \sum_{n=1}^N \Gamma_n \left(b_n \rho_R b_n^\dagger - \frac{1}{2} \{ b_n^\dagger b_n, \rho_R \} \right) \quad (\text{B2})$$

acting locally on each mode. The interaction term with the system has the form

$$H'_I := \sum_{k=1}^m A_{Sk} \otimes F_{Rk}, \quad (\text{B3})$$

where the interaction operators F_{Rk} of the environment are linear in the creation and annihilation operators:

$$F_{Rk} := \sum_{n=1}^N (c_{nk} b_n + c_{nk}^* b_n^\dagger). \quad (\text{B4})$$

Assuming factorizing initial conditions $\rho_0 = \rho_{0S} \otimes \rho_{0R}$ with $\rho_{0R} = \bigotimes_{n=1}^N |0\rangle\langle 0|_n$, which is Gaussian and stationary under this dynamics, meaning it satisfies

$$\mathcal{L}_R[\rho_{0R}] := -i[H_R, \rho_{0R}] + \mathcal{D}_R[\rho_{0R}] = 0,$$

the correlation function

$$C_{kk'}^R(t + \tau, \tau) := \langle F_{Rk}(t + \tau) F_{Rk'}(\tau) \rangle_R \quad (\text{B5})$$

is independent of the first evolution time τ . We will drop the τ time argument from now on and also restrict our analysis to a single interaction operator ($m = 1$ in Eq. (B3)), so in the following the correlation function (B5) will be denoted by $C^R(t)$. Writing it out explicitly in terms of the expression of F_R , we get

$$C^R(t) = \sum_{m,n=1}^N c_m c_n^* \langle b_m(t) b_n^\dagger(0) \rangle_R, \quad (\text{B6})$$

since terms with two creation or annihilation operators and contributions proportional to $\langle b_m^\dagger(t) b_n(0) \rangle_R$ are zero for our initial vacuum state.

It is easy to show that the hopping coupling constants g_n can be assumed real and positive without loss of generality in $C^R(t)$: define the canonical transformation

$$b_n \mapsto e^{i\delta_n} b_n \quad (\text{B7})$$

for arbitrary real δ_n . The creation operators b_n^\dagger will transform with the opposite phase, preserving the canonical commutation relations. The free term in the Hamiltonian (B1) and the dissipator (B2) are invariant under this transformation; the hopping term in Eq. (B1) and the interaction operator F_R defined as in (B4) are not:

$$\begin{aligned} c_n a_n + c_n^* b_n^\dagger &\mapsto c_n e^{i\delta_n} b_n + c_n^* e^{-i\delta_n} b_n^\dagger \\ g_n b_n b_{n+1}^\dagger + g_n^* b_n^\dagger b_{n+1} &\mapsto g_n e^{i(\delta_n - \delta_{n+1})} b_n b_{n+1}^\dagger \\ &\quad + g_n^* e^{-i(\delta_n - \delta_{n+1})} b_n^\dagger b_{n+1}. \end{aligned}$$

Taking δ_n such that $g_n e^{i(\delta_n - \delta_{n+1})} = |g_n|$, we may absorb the phase of the couplings in the still undetermined c_n , without restricting the physical picture in any way. Note that this leaves one of the δ_n still free as an overall phase in all the operator coefficients, which may be set e.g. so that c_1 or c_N is real.

The free dynamics of the oscillators with no coupling to the system is given by the Lindblad equation

$$\frac{d}{dt} \rho_R(t) = -i[H_R, \rho_R(t)] + \mathcal{D}_R[\rho_R(t)]. \quad (\text{B8})$$

Acting with the operator b_n from the left on both sides and taking the trace, we get

$$\frac{d}{dt} \langle b_n(t) \rangle_R = \sum_{m=1}^N M_{nm} \langle b_m(t) \rangle_R, \quad (\text{B9})$$

with

$$\begin{aligned} M_{nm} &:= \alpha_n \delta_{nm} - i(g_m \delta_{n, m+1} + g_{m-1} \delta_{n, m-1}) \\ &= \begin{pmatrix} \alpha_1 & -ig_1 & 0 & \dots & 0 \\ -ig_1 & \alpha_2 & \ddots & & \vdots \\ 0 & \ddots & \ddots & & 0 \\ \vdots & & & \alpha_{N-1} & -ig_{N-1} \\ 0 & \dots & 0 & -ig_{N-1} & \alpha_N \end{pmatrix}, \end{aligned} \quad (\text{B10})$$

where we have introduced the shorthand $\alpha_n := -\frac{\Gamma_n}{2} - i\Omega_n$. Eq. (B9) can be solved formally by diagonalizing the tridiagonal matrix M . Since M is not Hermitian, one has

$$M = S \Lambda S^{-1},$$

with $\Lambda := \text{diag}(\lambda_1, \dots, \lambda_N)$ the diagonal matrix containing the eigenvalues, $S := (\mathbf{u}^1, \dots, \mathbf{u}^N)$ a matrix made of arbitrarily normalized right eigenvectors \mathbf{u}^n and $S^{-1} := (\mathbf{v}^1, \dots, \mathbf{v}^N)^T$ its inverse, whose rows $(\mathbf{v}^n)^T$ are left eigenvectors. Since M is a symmetric matrix, left and right eigenvectors are the same, so S^{-1} is just the

transpose of S up to normalization of the rows in such a way that

$$\sum_{l=1}^N \mathbf{v}_l^m \mathbf{u}_l^n = \delta_{mn}.$$

Assuming that none of the eigenvalues are degenerate, which is always the case in numerical applications since the Λ matrices with equal diagonal elements are a zero-measure set, the evolution of the expectation value $\langle b_n(t) \rangle_R$ is thus

$$\begin{aligned} \langle b_n(t) \rangle_R &= \sum_{m=1}^N (S e^{\Lambda t} S^{-1})_{nm} \langle b_m(0) \rangle_R \\ &= \sum_{k,m=1}^N e^{\lambda_k t} \mathbf{u}_n^k \mathbf{v}_m^k \langle b_m(0) \rangle_R, \end{aligned} \quad (\text{B11})$$

and extends to the correlation functions $\langle b_n(t) b_m^\dagger(0) \rangle_R$ by the quantum regression hypothesis, which is true by construction in the context of Theorem 1 of the main text [57]; since $\langle b_n(0) b_m^\dagger(0) \rangle_R = \delta_{nm}$ on our initial state, one has

$$\langle b_n(t) b_m^\dagger(0) \rangle_R = \sum_{k=1}^N e^{\lambda_k t} \mathbf{u}_n^k \mathbf{v}_m^k, \quad (\text{B12})$$

which can now be substituted into (B6) to give the expression found in Eqs. (20) and (21) main text:

$$C^R(t) = \sum_{n=1}^N \left(\sum_{k,l=1}^N c_k c_l^* \mathbf{u}_k^n \mathbf{v}_l^n \right) e^{\lambda_n t}, \quad (\text{B13})$$

or

$$C^R(t) = \sum_{n=1}^N w_n e^{\lambda_n t} \quad (\text{B14})$$

in terms of the coefficients

$$w_n := \sum_{k,l=1}^N c_k c_l^* \mathbf{u}_k^n \mathbf{v}_l^n. \quad (\text{B15})$$

If degenerate eigenvalues λ_k^d are present, the time evolution in the corresponding subspace will be driven by $e^{\lambda_k^d t}$ times growing powers of t ; we did not consider this case for the sake of simplicity, but it may be useful to keep in mind that a mixed algebraic and exponential time dependence of correlation functions is not entirely ruled out by considering a Lindblad dynamics. If one wishes to explore this possibility in the TSO method, equality of two or more eigenvalues should be enforced at the level of the initial fit of the original correlation function $C^E(t)$ (see the next paragraph), since its spontaneous occurrence in the numerical procedure is virtually impossible.

2. Inversion problem from a given correlation function

To construct an effective environment whose $C^R(t)$ is as similar as possible to the $C^E(t)$ of a given unitary environment, we first fit $C^E(t)$ with a linear combination of N complex exponentials $e^{\tilde{\lambda}_n t}$ weighted by complex coefficients \tilde{w}_n , with N large enough to give an accurate fit, and then work backwards from Eq. (B14) to find the parameters that give the best approximation of the target function.

Since the real parameters in $C^R(t)$ are $4N - 1$ (taking into account the fact that $\sum_{n=1}^N w_n = \sum_{n=1}^N |c_n|^2$ is real and positive by construction) and it takes $5N - 2$ real parameters (N frequencies, N damping rates, $N - 1$ couplings and N complex coefficients c_n minus one overall redundant phase) to identify an effective environment, this is a highly nontrivial inversion problem, because the map from effective environments to correlation functions is both nonlinear and many-to-one. This means that existence or uniqueness of a solution to our problem are not guaranteed in general; furthermore, we must require $\Gamma_n > 0$ for all n in order for our effective master equation to be meaningful, which sets another important constraint.

It is useful to break down the problem into two parts: first an inverse eigenvalue problem leading from the λ_n to the dynamical matrix M , and then a system of equations relating the coefficients \tilde{w}_n to the interaction operator parameters c_n . This allows us to deal with the sign constraints on the rates once and for all in the first half of the solution procedure, and to exploit the fact that the c_n only appear in the second.

To determine the relation between the eigenvalues and elements of the matrix M , it is not convenient to look for symbolic expressions for each eigenvalue in terms of the parameters, since these would necessarily involve high-degree roots of complex polynomials. A simpler approach is to consider the characteristic polynomial of M

$$p_M(\lambda) := \det(\lambda \mathbb{I} - M) = \prod_{n=1}^N (\lambda - \lambda_n),$$

substitute the target eigenvalues $\tilde{\lambda}_n$ on the right-hand side and equate the coefficients of like powers of λ , which are geometrical invariants of any operator. The result is a system of equations of degrees 1 through N

$$\left\{ \begin{array}{l} \sum_{n=1}^N \alpha_n = \sum_{n=1}^N \tilde{\lambda}_n \\ \sum_{m \neq n}^N \alpha_m \alpha_n + \sum_{n=1}^{N-1} g_n^2 = \sum_{m \neq n}^N \tilde{\lambda}_m \tilde{\lambda}_n \\ \vdots \\ \det(M) = \prod_{n=1}^N \tilde{\lambda}_n \end{array} \right. \quad (\text{B16})$$

stating the invariance of the sums of principal minors order by order (the trace and the determinant appearing in the first and last equation being the simplest such invariants).

Now, Eq. (B16) can be regarded as a parametric system of equations in the couplings g_n . With the g_n fixed, it becomes an algebraic nonlinear system of N equations in N unknowns which can be solved numerically to give multiple sets of α_n —i.e. frequencies Ω_n and rates Γ_n whose sign can be checked directly—and therefore the entire dynamical matrix M .

Given a dynamical matrix M obtained by choosing some set of g_n and solving Eq. (B16), its eigenvectors \mathbf{u}^n and \mathbf{v}^n can be substituted into the w_n as defined in Eq. (B15), which then become functions of the c_n only and can be equated with the target values \tilde{w}_n

$$\begin{cases} \sum_{m,n=1}^N c_m^* \mathbf{v}_m^1 \mathbf{u}_n^1 c_n = \tilde{w}_1 \\ \vdots \\ \sum_{m,n=1}^N c_m^* \mathbf{v}_m^N \mathbf{u}_n^N c_n = \tilde{w}_N \end{cases} \quad (\text{B17})$$

to solve the second half of the problem. These N complex equations are equivalent to $2N - 1$ equations in $2N - 1$ real unknowns, since the overall phase of all c_n drops out of the left-hand side while on the right-hand side $\sum_{n=1}^N \tilde{w}_n = C^E(0)$ has no imaginary part.

A set of c_n solving Eq. (B17) does not always exist, so here we numerically minimize the Manhattan distance between the w_n on the left-hand side and the \tilde{w}_n instead. At this point, we have converted an arbitrary $(N - 1)$ -tuple of coupling constants into a trial effective correlation function

$$C_{\text{trial}}^R(t) = \sum_{n=1}^N w_n(g_m, \alpha_m, c_m) e^{\lambda_n(g_m, \alpha_m)t}$$

which can be compared to the target $C^E(t)$ according to some figure of merit. We used the integral

$$I_1(t_{\text{max}}) := \int_0^{t_{\text{max}}} dt' \int_0^{t'} dt'' |C_{\text{trial}}^R(t' - t'') - C^E(t' - t'')| \quad (\text{B18})$$

up to some final time t_{max} such that $C^E(t_{\text{max}}) \ll 1$ in all cases where we had a closed expression for it, and

$$I_2(t_{\text{max}}) := \Delta t \sum_{n=1}^{N_{\text{max}}} |C_{\text{trial}}^R(n\Delta t) - C^E(n\Delta t)| \quad (\text{B19})$$

for some number of points N_{max} and timestep $\Delta t = t_{\text{max}}/N_{\text{max}}$ when $C^E(t)$ was only known in integral form and needed to be evaluated for each value of the time argument. This whole procedure can be carried out for many values of the couplings in the physical parameter region, ranking the corresponding trial correlation functions by

their values of the figure of merit in search of an optimum, in the spirit of the error bounds in [45] which relate the absolute difference between correlation functions to the changes in the reduced dynamics.

To summarize the steps described above, in order to find an effective environment corresponding to some correlation function $C^E(t)$, we first fit it with complex exponentials, and then overcome the mismatch between the number of variables from this fit and the number of parameters in the effective environment by setting up a variational problem in the g_n couplings between neighboring surrogate modes. We sample multiple $(N - 1)$ -tuples (g_1, \dots, g_{N-1}) in a suitably sized open set $(0, g_{\text{max}})^{N-1}$, solve Eq. (B16) for each of them and then plug the eigenvectors of all physically acceptable matrices M found into Eq. (B17) to determine the c_n . The trial correlation functions $C_{\text{trial}}^R(t)$ constructed from each set of parameters are ranked according to the estimators (B18) or (B19), depending on the original $C^E(t)$, and we search for the minimum of the figure of merit in the space of the g_n .

This variational problem is not convex in general: both the shape of the region in g_n -space leading to physically admissible solutions and the dependence of the cost functions defined in Eqs. (B18) and (B19) on the couplings can be highly nontrivial, with trenches, pointed features, local minima and gaps without any solutions at all appearing at unpredictable locations. We have also found no obvious patterns giving any hints as to the existence of a region of physically acceptable values of g_n (for any N) such that there are exact solutions, or the form that such a region may have, based on the target parameters. All these mathematical features are very model-dependent; Fig. 11 shows some examples of parameter space shapes and cost function behavior for different correlation functions approximated using $N = 3$ surrogate oscillators. Though none of the examples shown gave a $C^R(t)$ of sufficient accuracy for practical use due to the small number of effective modes, they nonetheless give a clear qualitative idea of the variety of possible outcomes. In general, sampling the parameter space efficiently is difficult, and we are looking for ways to improve this part of the algorithm.

Appendix C: Special cases with exact solutions

We will now show some examples, both general and related to the specific systems treated in the main text, of analytical solutions of the inversion problem in specific cases.

1. One and two oscillators

The simplest possible effective environment is a single damped oscillator ($N = 1$ in Eq. (B1), with interaction operator $F_R = c(b + b^\dagger)$ since the phase of c can be set to

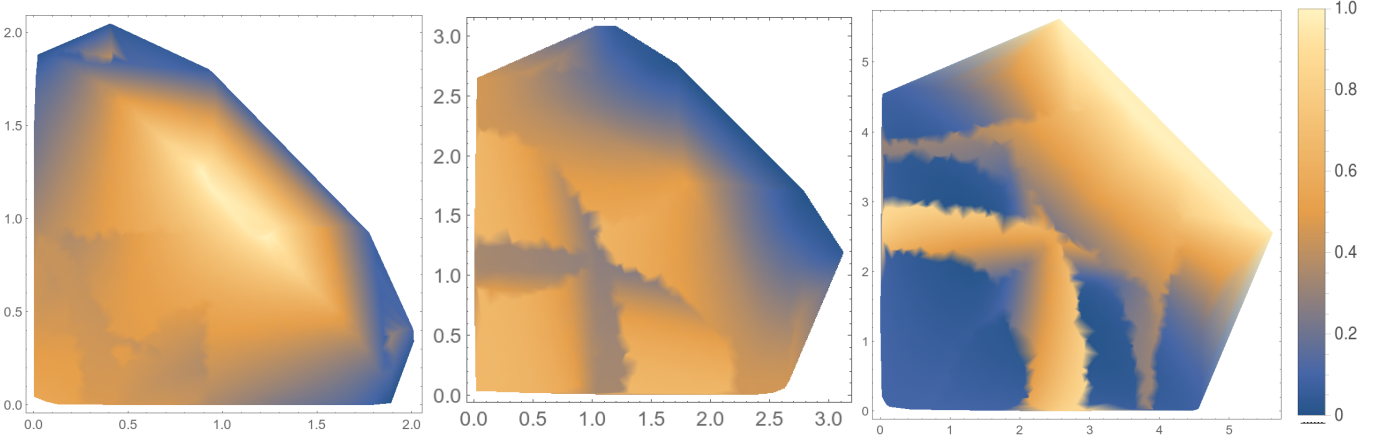


Figure 11: Shape of the space of g_n such that all Γ_n are positive, with $N = 3$ and three different thermal correlation functions $C_\beta^E(t)$ corresponding to $J(\omega) = \omega e^{-\omega/\Omega_c}$, $J(\omega) = (\omega^2/\Omega_c)e^{-\omega/\Omega_c}$ and $J(\omega) = (\omega^5/\Omega_c^4)e^{-\omega/\Omega_c}$, all at $\beta\Omega_c = 0.85$. The axes show the values of g_1 and g_2 and the color denotes accuracy of the trial correlation function as estimated by $I_1(t_{\max})$ with $\Omega_c t_{\max} = 25$ and normalized to the maximum accuracy obtained for each case, with blue areas representing smaller errors and yellow and orange ones indicating very vague resemblance.

zero). This yields a correlation function

$$C^R(t) = c^2 e^{-\frac{\Gamma}{2}|t| - i\Omega t}$$

where the time dependence at $t < 0$ is defined by $C^R(-t) := C^{R*}(t)$ because the Lindblad equation only gives $C^R(t)$ for positive times, as discussed in Section III of the main text. The Fourier transform of this function is a Lorentzian of width Γ centered in Ω :

$$C^R(\omega) = c^2 \frac{\Gamma}{(\Gamma/2)^2 + (\omega - \Omega)^2}.$$

A single sharp peak at zero temperature in the target spectral density can be mapped to a mode like this by simple nonlinear fitting of $C^E(t)$ with a complex exponential, as we did for the dimer simulations in Section V of the main text: in that case, the peaks were antisymmetrized Lorentzians so the frequency and damping rate of the effective mode matched those from the original spectral density almost exactly.

A less trivial, still exactly solvable case is given by two interacting oscillators and was already introduced by Garraway in [48] to show that not only sums but also differences of Lorentzians can be modeled by pseudomodes. In that paper, only one of the modes is coupled to the system (i.e. $c_2 = 0$); here we lift this assumption to show a more general result.

The general correlation function for $N > 1$ has the form

$$C^R(t) = \sum_{n=1}^N w_n e^{\lambda_n t} \quad (\text{C1})$$

with $\Re[\lambda_n] < 0$, where the fact that the w_n are complex changes the form in the frequency domain from a simple

linear combination of Lorentzians to

$$C^R(\omega) = -2 \sum_{n=1}^N \frac{\Re[w_n] \Re[\lambda_n] + \Im[w_n] (\omega + \Im[\lambda_n])}{\Re[\lambda_n]^2 + (\omega + \Im[\lambda_n])^2}, \quad (\text{C2})$$

thus adding a linear frequency dependence in the numerator of the term associated with each mode. In phenomenological approaches where there is no intention of accurately simulating a specific correlation function, one may use ad-hoc combinations of weights and exponents to cancel terms in the numerator of the full $C^R(\omega)$ written as a single fractional polynomial and achieve a steeper fall-off in frequency than is possible with individual Lorentzians with positive coefficients (again, one example is given in [48]). Such strategies hardly generalize beyond specific applications but can be helpful to mitigate the error associated with the behavior of $C^R(\omega)$ near the origin, which does not comply with the fluctuation-dissipation theorem in general, as discussed in the main text.

In the case $N = 2$, the eigenvalues $\lambda_{1,2}$ and weights $w_{1,2}$ depend on the effective environment parameters through the relations

$$\begin{aligned} \lambda_{1,2}(\alpha_{1,2}, g) &= \frac{\alpha_1 + \alpha_2}{2} \pm \sqrt{\left(\frac{\alpha_1 - \alpha_2}{2}\right)^2 - g^2} \\ w_{1,2}(\alpha_{1,2}, g, c_{1,2}) &= \frac{|c_1|^2 + c_2^2}{2} \\ &\quad \pm \frac{(|c_1|^2 - c_2^2)(\alpha_1 - \alpha_2) - 4ig\Re[c_1]c_2}{2\sqrt{(\alpha_1 - \alpha_2)^2 - 4g^2}}, \end{aligned} \quad (\text{C3})$$

where c_2 is taken to be real by fixing the overall phase mentioned in the preceding section. The first equations

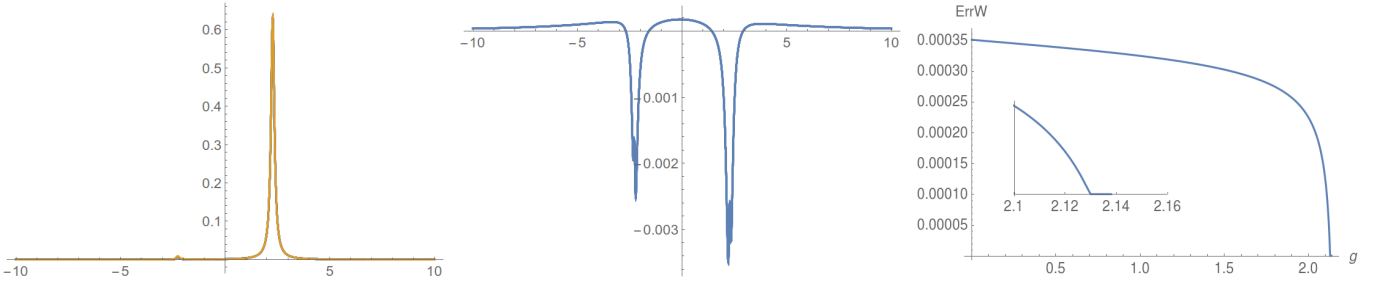


Figure 12: Left to right: overlapping plots of $C_\beta^E(\omega)$ and the effective $C_\beta^R(\omega)$ with $N = 2$ for an antisymmetrized Lorentzian with peak frequency $\Omega_{AL} = 2.15u$ and width $\Gamma_{AL} = 0.1u$ in units $u = 100 \text{ cm}^{-1}$, at temperature $T = 77 \text{ K}$; a plot of the difference $C_\beta^E(\omega) - C_\beta^R(\omega)$; a plot of the minimum Manhattan distance $\sum_{n=1}^N |\tilde{w}_n - w_n|$ as a function of g , with a very small region around $g = 2.14u$ (shown in the inset) in which the \tilde{w}_n can only just be matched exactly, before the Γ_n in the solutions change sign and higher values of g no longer give acceptable solutions. Notice both the very steep descent of the error and the abrupt end of the physically admissible region on either side of this spot, as an example of how minima in our figures of merit quickly become hard to find in a more coarse-grained sampling in higher dimensions.

is readily inverted parametrically in g :

$$\alpha_{1,2} = \frac{\tilde{\lambda}_1 + \tilde{\lambda}_2}{2} \pm \sqrt{\left(\frac{\tilde{\lambda}_1 - \tilde{\lambda}_2}{2}\right)^2 + g^2}. \quad (\text{C4})$$

The domain of physically admissible solutions is the set of all g such that $\Gamma_{1,2} = -2\Re[\alpha_{1,2}] > 0$ and can be found by using the formula for the square root of a complex number $z = z_R + iz_I$

$$\sqrt{z} = \sqrt{\frac{|z| + z_R}{2}} + i \operatorname{sgn}(z_I) \sqrt{\frac{|z| - z_R}{2}}.$$

Using Eq. (C4) in the equation for the weights, this becomes parametric in g as well:

$$\tilde{w}_{1,2} = \frac{|c_1|^2 + c_2^2}{2} \mp \frac{(|c_1|^2 - c_2^2) \sqrt{(\tilde{\lambda}_1 - \tilde{\lambda}_2)^2 + 4g^2} - 4ig\Re[c_1]c_2}{2(\tilde{\lambda}_1 - \tilde{\lambda}_2)}. \quad (\text{C5})$$

This equation, which relates the four real quantities g , $\Re[c_1]$, $\Im[c_1]$ and c_2 to the three real numbers determining $\tilde{w}_{1,2}$, may or may not have a solution depending on the g chosen, as discussed earlier: if the solution exists only for g outside the physical region in which $\Gamma_{1,2} = -2\Re[\alpha_{1,2}] > 0$, then it is necessary to operate variationally and minimize the distance $\sum_{n=1}^2 |\tilde{w}_n - w_n(\alpha_{1,2}, g, c_{1,2})|$.

If one assumes $c_2 = 0$ in (C3), as is done in [48], then the whole system can be inverted explicitly:

$$\left\{ \begin{array}{l} |c_1|^2 = \tilde{w}_1 + \tilde{w}_2 \\ \alpha_1 = \frac{\tilde{w}_1 \tilde{\lambda}_1 + \tilde{w}_2 \tilde{\lambda}_2}{\tilde{w}_1 + \tilde{w}_2} \\ \alpha_2 = \frac{\tilde{w}_1 \tilde{\lambda}_2 + \tilde{w}_2 \tilde{\lambda}_1}{\tilde{w}_1 + \tilde{w}_2} \\ g^2 = \left(\frac{\tilde{\lambda}_1 - \tilde{\lambda}_2}{2}\right)^2 \left(\left(\frac{\tilde{w}_1 - \tilde{w}_2}{\tilde{w}_1 + \tilde{w}_2}\right)^2 - 1 \right) \end{array} \right. \quad (\text{C6})$$

but the solution only exists if the $\tilde{\lambda}_{1,2}$, $\tilde{w}_{1,2}$ given are such that the expression on the right-hand side of the last equation has a vanishing imaginary part. This is because now the phase of c_1 has also decoupled from the problem, removing a second real degree of freedom and making the system overdetermined: the balance between equations and unknowns is thus restored by this real constraint appearing on the $\tilde{\lambda}_{1,2}$, $\tilde{w}_{1,2}$.

In our applications, we used pairs of effective modes to reproduce narrow antisymmetrized Lorentzians at nonzero temperature: we found no exact solution and had to minimize $\sum_{n=1}^2 |\tilde{w}_n - w_n(\alpha_{1,2}, g, c_{1,2})|$ in most cases, but e.g. for an antisymmetrized Lorentzian with peak frequency $\Omega_{AL} = 215 \text{ cm}^{-1}$ and width $\Gamma_{AL} = 10 \text{ cm}^{-1}$ at temperature 77 K the system can be solved exactly for $213.0 \text{ cm}^{-1} < g < 213.8 \text{ cm}^{-1}$ (Fig. 12). Note that in all cases we considered, the best fit of such thermalized peaks with two modes was always obtained by mode frequencies close to zero and a strong coupling g between the two; fitting the same function with two noninteracting modes at the positive and negative peak frequencies was consistently found to be a less accurate choice even for such seemingly obvious target functions.

2. Three oscillators

Adding a third oscillator, we found exact solutions for $c_2 = 0$, which we did not use in any of the simulations discussed in the main paper but can be useful in general.

For $N = 3$, the system of eigenvalue equations is

$$\left\{ \begin{array}{l} \alpha_1 + \alpha_2 + \alpha_3 = \tilde{\lambda}_1 + \tilde{\lambda}_2 + \tilde{\lambda}_3 \\ \alpha_1 \alpha_2 + \alpha_2 \alpha_3 + \alpha_3 \alpha_1 + g_1^2 + g_2^2 = \tilde{\lambda}_1 \tilde{\lambda}_2 + \tilde{\lambda}_2 \tilde{\lambda}_3 + \tilde{\lambda}_3 \tilde{\lambda}_1 \\ \alpha_1 \alpha_2 \alpha_3 + g_1^2 \alpha_1 + g_2^2 \alpha_3 = \tilde{\lambda}_1 \tilde{\lambda}_2 \tilde{\lambda}_3 \end{array} \right. \quad (\text{C7})$$

and one may remove α_2 from the last two equations by using the first, so that α_1 and α_3 can be regarded as

effective functions of the real parameters g_1 and g_2 .

With c_2 set to zero, the whole inversion problem is determined, since the equations for the \tilde{w}_n will determine the values of g_1 and g_2 instead. Setting the overall phase so that c_3 is real, the equations can be written as

$$\left\{ \begin{array}{l} |c_1|^2 + c_3^2 = \tilde{w}_1 + \tilde{w}_2 + \tilde{w}_3 \\ |c_1|^2 \alpha_1 + c_3^2 \alpha_3 = \tilde{w}_1 \tilde{\lambda}_1 + \tilde{w}_2 \tilde{\lambda}_2 + \tilde{w}_3 \tilde{\lambda}_3 \\ 2\Re[c_1] c_3 g_1 g_2 = -\tilde{w}_3 (\tilde{\lambda}_1 - \tilde{\lambda}_3) (\tilde{\lambda}_2 - \tilde{\lambda}_3) \\ \quad - \frac{(\alpha_1 - \tilde{\lambda}_1)(\alpha_1 - \tilde{\lambda}_2)(\alpha_3 - \tilde{\lambda}_3)}{(\alpha_3 - \alpha_1)(\alpha_1 - \tilde{\lambda}_3)} |c_1|^2 \\ \quad - \frac{(\alpha_3 - \tilde{\lambda}_1)(\alpha_3 - \tilde{\lambda}_2)(\alpha_1 - \tilde{\lambda}_3)}{(\alpha_3 - \alpha_1)(\alpha_3 - \tilde{\lambda}_3)} c_3^2 \end{array} \right. \quad (\text{C8})$$

where the last line again features a real expression on the left-hand side and a complex one whose imaginary part must be zero on the right-hand side. Since the first equation is real by construction, there are five real equations in the five real variables $g_1, g_2, \Re[c_1], \Im[c_1], c_3$

in Eq. (C8), so the existence of solutions is only subject to the constraint $\Gamma_n = -2\Re[\alpha_n] > 0$.

If c_3 is also set to zero, then the system (C8) becomes

$$\left\{ \begin{array}{l} c_1^2 = \tilde{w}_1 + \tilde{w}_2 + \tilde{w}_3 \\ c_1^2 \alpha_1 = \tilde{w}_1 \tilde{\lambda}_1 + \tilde{w}_2 \tilde{\lambda}_2 + \tilde{w}_3 \tilde{\lambda}_3 \\ 0 = -\tilde{w}_3 (\tilde{\lambda}_1 - \tilde{\lambda}_3) (\tilde{\lambda}_2 - \tilde{\lambda}_3) \\ \quad - \frac{(\alpha_1 - \tilde{\lambda}_1)(\alpha_1 - \tilde{\lambda}_2)(\alpha_3 - \tilde{\lambda}_3)}{(\alpha_3 - \alpha_1)(\alpha_1 - \tilde{\lambda}_3)} c_1^2. \end{array} \right. \quad (\text{C9})$$

and can be inverted explicitly, giving c_1^2, α_1 and α_3 . But now the system (C7) is overdetermined: the trace gives α_2 , and the last two complex equations can give $g_{1,2}$ only if the $\tilde{\lambda}_n$ and \tilde{w}_n happen to satisfy two real relations among themselves (one because c_3 was removed from the problem, another because the phase of c_1 is now irrelevant). In particular, the expressions whose imaginary part must vanish now appear on the right-hand side of the last two lines of the full solution

$$\left\{ \begin{array}{l} c_1^2 = \tilde{w}_1 + \tilde{w}_2 + \tilde{w}_3 \\ \alpha_1 = \frac{\tilde{w}_1 \tilde{\lambda}_1 + \tilde{w}_2 \tilde{\lambda}_2 + \tilde{w}_3 \tilde{\lambda}_3}{\tilde{w}_1 + \tilde{w}_2 + \tilde{w}_3} \\ \alpha_2 = \frac{(\tilde{w}_2 + \tilde{w}_3) \tilde{\lambda}_1 + (\tilde{w}_3 + \tilde{w}_1) \tilde{\lambda}_2 + (\tilde{w}_1 + \tilde{w}_2) \tilde{\lambda}_3}{\tilde{w}_1 + \tilde{w}_2 + \tilde{w}_3} \\ \quad - \frac{\tilde{w}_2 \tilde{w}_3 (\tilde{\lambda}_2 - \tilde{\lambda}_3)^2 \tilde{\lambda}_1 + \tilde{w}_3 \tilde{w}_1 (\tilde{\lambda}_3 - \tilde{\lambda}_1)^2 \tilde{\lambda}_2 + \tilde{w}_1 \tilde{w}_2 (\tilde{\lambda}_1 - \tilde{\lambda}_2)^2 \tilde{\lambda}_3}{\tilde{w}_2 \tilde{w}_3 (\tilde{\lambda}_2 - \tilde{\lambda}_3)^2 + \tilde{w}_3 \tilde{w}_1 (\tilde{\lambda}_3 - \tilde{\lambda}_1)^2 + \tilde{w}_1 \tilde{w}_2 (\tilde{\lambda}_1 - \tilde{\lambda}_2)^2} \\ \alpha_3 = \frac{\tilde{w}_2 \tilde{w}_3 (\tilde{\lambda}_2 - \tilde{\lambda}_3)^2 \tilde{\lambda}_1 + \tilde{w}_3 \tilde{w}_1 (\tilde{\lambda}_3 - \tilde{\lambda}_1)^2 \tilde{\lambda}_2 + \tilde{w}_1 \tilde{w}_2 (\tilde{\lambda}_1 - \tilde{\lambda}_2)^2 \tilde{\lambda}_3}{\tilde{w}_2 \tilde{w}_3 (\tilde{\lambda}_2 - \tilde{\lambda}_3)^2 + \tilde{w}_3 \tilde{w}_1 (\tilde{\lambda}_3 - \tilde{\lambda}_1)^2 + \tilde{w}_1 \tilde{w}_2 (\tilde{\lambda}_1 - \tilde{\lambda}_2)^2} \\ g_1^2 = -\frac{\tilde{w}_2 \tilde{w}_3 (\tilde{\lambda}_2 - \tilde{\lambda}_3)^2 + \tilde{w}_3 \tilde{w}_1 (\tilde{\lambda}_3 - \tilde{\lambda}_1)^2 + \tilde{w}_1 \tilde{w}_2 (\tilde{\lambda}_1 - \tilde{\lambda}_2)^2}{(\tilde{w}_1 + \tilde{w}_2 + \tilde{w}_3)^2} \\ g_2^2 = -\frac{\tilde{w}_1 \tilde{w}_2 \tilde{w}_3 (\tilde{\lambda}_2 - \tilde{\lambda}_3)^2 (\tilde{\lambda}_3 - \tilde{\lambda}_1)^2 (\tilde{\lambda}_1 - \tilde{\lambda}_2)^2 (\tilde{w}_1 + \tilde{w}_2 + \tilde{w}_3)}{(\tilde{w}_2 \tilde{w}_3 (\tilde{\lambda}_2 - \tilde{\lambda}_3)^2 + \tilde{w}_3 \tilde{w}_1 (\tilde{\lambda}_3 - \tilde{\lambda}_1)^2 + \tilde{w}_1 \tilde{w}_2 (\tilde{\lambda}_1 - \tilde{\lambda}_2)^2)^2}. \end{array} \right. \quad (\text{C10})$$